

Elemental thin film depth profiles by ion beam analysis using simulated annealing - a new tool

C.Jeynes^a, N.P.Barradas^b, P.K.Marriott^c, G.Boudreault^a, M.Jenkin^d, E.Wendler^e, R.P.Webb^a

a: University of Surrey Ion Beam Centre, Guildford, England
b: Instituto Tecnológico e Nuclear, E.N. 10, Sacavém, Portugal
c: Department of Statistics, National University of Singapore, Singapore
d: School of Electronics Computing and Mathematics, University of Surrey, Guildford, England
e: Friedrich-Schiller-Universität Jena, Institut für Festkörperphysik, Jena, Germany

Short Title: The DataFurnace - IBA depth profiles by simulated annealing

Abstract

Rutherford backscattering spectrometry and related techniques have long been used to determine the elemental depth profiles in films a few nms to a few microns thick. However, although obtaining spectra is very easy, solving the inverse problem of extracting the depth profiles from the spectra is not possible analytically except for special cases. It is because these special cases include important classes of samples, and because skilled analysts are adept at extracting useful qualitative information from the data, that ion beam analysis is still an important technique.

We have recently solved this inverse problem using the simulated annealing algorithm. We have implemented the solution in the "IBA DataFurnace" code, which has been developed into a very versatile and general new tool that analysts can now use to rapidly extract quantitative accurate depth profiles from real samples on an industrial scale. We review the features, applicability and validation of this new code together with other approaches to handling IBA (ion beam analysis) data, with particular attention being given to determining both the absolute accuracy of the depth profiles and statistically accurate error estimates.

We include a discussion of analyses using RBS, non-Rutherford elastic scattering, elastic recoil detection and non-resonant nuclear reactions. (PIXE - particle induced X-ray emission - is not discussed since it is hard to use it for depth profiling, and it is not implemented in DataFurnace.) Examples are discussed using multiple techniques simultaneously, high depth resolution, and where there is systematic ambiguity in the collected data. Analyses are shown: of evaporated, sputtered, oxidised, ion implanted, ion beam mixed and annealed materials; of semiconductors, optical and magnetic multilayers, superconductors, tribological films and metals; and of oxides on Si, mixed metal silicides, boron nitride, GaN, SiC, mixed metal oxides, YBCO and polymers.

Keywords: Inverse problems, turnkey analysis, Markov chain Monte Carlo, Bayesian statistics, DataFurnace

Elemental thin film depth profiles by ion beam analysis using simulated annealing - a new tool

Contents

1	Overview	3
2	Introduction to Ion Beam Analysis	3
3	The IBA Inverse Problem	6
4	Introduction to Simulated Annealing	8
5	Mixed Metal Silicides	10
6	Simulated Annealing: Algorithmic Issues	15
7	The Forward Model	17
8	Forward Model Limitations: Multiple Scattering	21
9	Ambiguity in IBA data: Multiple Spectra	22
10	Ambiguity in IBA data: Restricting the State Space	25
11	Examples of ERD	28
12	Precise IBA: Quantifying the Error by Bayesian Techniques	28
13	High Resolution RBS: A Proper Treatment of SiGe Multilayers	32
14	Non-resonant NRA	36
15	Accurate IBA	39
16	Forward Model Extension: Roughness	42
17	Forward Model Limitations: Stopping Powers (Optical Multilayers)	44
18	Other Examples	45
19	Future Developments: Turnkey IBA	46
20	Future Developments: The Algorithm and the Forward Model	47
21	Summary	49
	Acknowledgments	49
	Figures	49
	References	50

1-Overview

We will review our recent developments in thin film depth profiling with Ion Beam Analysis (IBA) in the context of the work of the community, discussing the scientific implications of these developments, which are such as to effectively establish a new depth profiling tool. We start with a simplified overview of IBA since we believe that our new tool will make IBA attractive to many users for the first time.

The essence of this new tool is its solution of the “inverse problem” of automatically extracting depth profiles from Rutherford backscattering (RBS) data: we therefore start with a description of this inverse problem and continue with an introduction to the Simulated Annealing algorithm on which the inverse problem's solution is built. This algorithm was first applied to RBS in 1997 by Barradas, Jeynes & Webb. After some RBS examples exemplifying the scope of the tool we give details of the physics (the "forward model") and the algorithm used. We describe and discuss the intrinsic ambiguity of IBA data and the systematic approaches to valid analysis in the presence of this ambiguity. We also show a number of examples using a variety of forward recoil techniques.

It is one of the major benefits of this new tool that the determination of the confidence limits on the calculated depth profiles can be done as a natural extension of the algorithm. We discuss the precision that is available in this way.

We also discuss the use of accurate calculations of energy resolution as a function of depth to enable us to do very high depth resolution analysis. Both of these features are used in the analysis of both SiGe multilayers analysed with RBS and deuterated polymer multilayers analysed with NRA (nuclear reaction analysis).

The accuracy of an analysis is in the end the most important issue. The establishment of a new tool depends first of all on being able to demonstrate that the answers are correct. At last a *routine* analysis of non-trivial samples is available which is both complete and at state of the art accuracy. Accuracy of analysis depends ultimately on the accuracy of the forward model: we end with a subtle discussion of limitations of the current forward model in the context of an extraordinarily precise analysis of an optical multilayer sample.

Finally we draw some conclusions and point out possible future developments. We have illustrated the review with a number of striking examples showing the wide range of types of samples that can be analysed and the wide variety of techniques that are supported with this general purpose tool.

2- Introduction to Ion Beam Analysis

IBA is a cluster of techniques involving materials analysis by MeV ion beams. When an energetic ion strikes a target there are a variety of energy loss mechanisms, any (or all) of which can be used (together or separately) to obtain information about the target. Table 1 summarises these techniques, and indicates those for which DataFurnace can be used to obtain elemental depth profiles.

Table 1: Glossary of IBA Techniques

Technique		Explanation	Data-Furnace?
RBS	Rutherford backscattering	Nuclear Coulomb scattering, incident ion is detected ($Q = 0$)	Yes
EBS	elastic (non-Rutherford) backscattering	Nuclear scattering as RBS, but where the Coulomb barrier is exceeded ($Q = 0$)	Yes
ERD	elastic recoil detection	Synonym for FRS ($Q = 0$)	Yes
FRS	forward recoil spectrometry	Synonym for ERD As RBS (or EBS) but where recoiled target atom is detected. This has to be in a forward scattering direction for kinematical reasons.	Yes
NRA	nuclear reaction analysis	Non-elastic interaction ($Q \neq 0$). Resultant reaction product detected (usually proton, alpha or deuterium)	Yes
PIXE	particle induced X-ray emission	X-rays from inelastic collisions of the incident ion with inner core electrons are easy to detect: similar spectra to EDAX	No
PIGE	particle induced gamma ray emission	Special case of NRA, where a photon is detected	No
channelling		Used with any IBA technique for quantifying and profiling damage in single crystal samples	No
microbeam		the ion beam can be focussed and scanned and used as a scanning ion microscope. RBS and other spectra can be collected from specific regions of the sample. Usually used with PIXE.	Yes
IL	ionoluminescence	as PIXE, but lower energy photons detected	No
IBIC	ion beam induced current	microbeam technique for investigating semiconductor devices, which respond to single ion impacts	No
STIM	scanning transmission ion microscopy	detects energy loss of single ions penetrating (relatively) thick targets.	No

IBA is now a mature scientific technique, very widely used in electronic materials research, and throughout thin film science: the most useful single volume overviews are in the Handbooks (Mayer & Rimini, 1977; Tesmer & Nastasi, 1995). It is a very large and diverse field which we do not intend to review here, only making a few general comments that may be useful for readers not analysts themselves. These readers should note that practitioners will probably quibble with almost all of our generalisations here which are intended only to allow newcomers to grasp IBA in a concrete way.

The first of the international biennial Ion Beam Analysis Conference series was held in 1973 (Mayer & Ziegler, 1973): these are now very large meetings, IBA-14 (Möller *et al*, 2000) had 362 participants and is supplemented by several other international conference series: both PIXE (see Malmqvist, 1999) and the microbeam (see Prozesky *et al*, 1999) have their own large conferences and there are many regional meetings. IBA is ubiquitous in the scientific thin film community: for example, IBA was used in 38% of the papers published at a recent IBMM (conference on the ion beam modification of materials: Vredenberg *et al*, 1999). And not only the materials community: for example, the Louvre Museum in Paris has its own dedicated accelerator (Amsel *et al*, 1990), and there is extensive international application of IBA techniques to cultural and archaeological artefacts (see Respaldiza & Gómez-Camacho, 1997).

IBA uses incident beam energies ranging perhaps from 100keV to 200MeV. At the low energy end the detectors become very expensive, as do the accelerators at the high end: we will not

attempt to summarise all the detectors and accelerators in use today. IBA really started when nuclear physics groups looked for new uses for their obsolete little 2MV Van de Graaff accelerators in the 1960s and 1970s, and there are still some of these machines around. The typical machine being installed today is a 2MV tandem machine which can deliver multiply charged beams up to perhaps 10MeV.

An ion beam striking a solid target has many types of interaction, any of which can be used for analysis. We should point out that nothing prevents the analyst installing multiple detectors in the target chamber to detect any or all of these interactions simultaneously.

Ionoluminescence has the highest cross-section of all the interactions: this is a very young field (see for example Bettioli *et al*, 1994, and Yang *et al*, 1994). PIXE (particle induced X-ray emission: see Johanssen & Campbell, 1988) typically uses a 3MeV proton beam, although He is also used. It is directly comparable with electron probe microanalysis (EPMA) with very similar spectra, except that there is negligible primary bremsstrahlung background due to the much higher particle mass. PIXE therefore has much higher sensitivity than EPMA. Cross-sections can be hundreds of barns ($1 \text{ barn} = 10^{-24} \text{ cm}^2$).

RBS (Rutherford backscattering, see Chu *et al*, 1978) typically uses a 2MeV He beam with typical cross-sections of a barn: but for a similar energy proton beam the Coulomb barrier of light target nuclei (up to P) is exceeded and the cross-sections are no longer Rutherford although the interactions may remain elastic. We call this EBS (elastic non-Rutherford backscattering). EBS cross-sections can exceed RBS ones by orders of magnitude. Of course, two body interactions between the incident ion and the target nucleus will both scatter the ion and recoil the target nucleus into forward directions. The recoils carry much information about the sample and can also be detected. This is known variously as FRS (forward recoil spectroscopy) or ERD (elastic recoil detection, see Tirara *et al*, 1996).

Where the interaction energy is sufficiently high the nuclear structure becomes involved, the interaction may become inelastic, and nuclear reactions can occur: NRA (nuclear reaction analysis) is often very useful since it is isotope specific and there is often no background to the signal, but cross-sections typically fall by orders of magnitude (Vizkelethy, 1995; Hirvonen, 1995).

Turning to beam and sample manipulation, *microbeams* as small as 50nm have been formed, and 1 micron microbeams are in widespread routine use: thus lateral maps of the major, minor and trace elements of the sample are readily available by PIXE (see Watt & Grime, 1987). Note that for PIXE the excitation volume where the X-rays are generated is essentially determined by the beam spot size since protons are not deflected much by electrons. In contrast, the excitation volume for X-ray analysis in the SEM is determined by the electron beam energy, and is often larger than 5 microns across. Therefore PIXE X-ray maps are typically of much higher lateral resolution than EPMA ones. Of course, secondary *electron* maps are of much lower resolution for PIXE than for the SEM.

High energy ion beams can be very well collimated and aligned with symmetry directions in single crystal samples, making lattice site and damage information available. Known as *channelling*, this is a very large field in its own right (see Feldman *et al*, 1982; Götz & Gärtner, 1988). Other interesting emerging fields include *in situ* observation of the electrical behaviour of working semiconductor devices by ion beam induced current (IBIC: see for example Breese,

Amaku & Wilshaw, 1998), and the characterisation of the defect structure of thick crystalline samples using a channelled beam in transmission (STIM: scanning transmission ion microscopy, see for example Breese, King & de Kerckhove, 1998).

We emphasise that the IBA DataFurnace we describe applies *only* to thin film composition depth profiling and *not* to the various microbeam imaging or channelling applications. Also, we have not yet implemented PIXE although this is often a very useful complementary technique (see for example Loh *et al*, 1993).

3- The IBA Inverse Problem

Rutherford scattering: In 1911 Ernest Rutherford explained the structure of the atom as a positively charged nucleus surrounded by electrons, where the nucleus was tiny with respect to the size of the atom (already known then to be around 1Å). He used a simple Coulomb potential and contradicted J.J.Thompson's "pudding" model. Rutherford based his model on Geiger and Marsden's (1909) data on the "diffuse scattering" (in backward directions) of alpha particles by metal foils, and Geiger's (1910) data on the most probable angle of scattering of transmitted particles. Although the most probable scattering angle is very low, indicating a distributed charge as in Thompson's model, backscattering events require a concentrated charge at the centre of the atom (requiring the concept of the nucleus). Geiger and Marsden (1913) subsequently verified Rutherford's calculation of the scattering probability, or *cross-section*.

Elemental Depth Profiles: It turns out that simple silicon diodes very conveniently stop alphas of MeV energies, converting their energy into a cloud of electron-hole pairs which can be separated by the electric field if the diode is reverse biased. High quality electronics to determine the number of electrons arriving at the anode, and hence the *energy* of the particle, have been available for over three decades. These detectors are effectively 100% efficient, detecting every particle that strikes them. Thus an alpha scattering experiment can determine the *mass* of the target nucleus (from the energy of the scattered alpha, using the *kinematics*: conservation of energy and momentum), the *depth* of the target nucleus (also from the energy of the scattered alpha, this time using the *energy loss* as a function of depth in the target material), and the *concentration* of the target nucleus (from the absolute number of scattered alphas, using the cross-sections that Rutherford calculated).

Mass-Depth Ambiguity: Rutherford backscattering spectrometry (RBS) can therefore, in principle, determine the complete elemental depth profile of a sample from the energy spectrum of the scattered particles. However, the reader will have noticed that the scattered particle energy is a function both of the mass of the target nucleus, and of the depth of the target nucleus in the sample. This ambiguity in the interpretation of the detected particle energy is the origin of the *inverse problem* that is at the heart of this paper.

Brice (1973) has shown that the elastic backscattering spectrum has the form of a triple integral:

$$\Psi_e(E, E_3) = A \frac{\partial}{\partial E_3} \int_0^\infty dx' \int_0^t N_e dx \int_{E'}^E dE_1 P_{in} P_{out} \sigma(E_1)/S(E_1) \quad (1)$$

where Ψ_e is the number of incident particles energy E backscattered with energy E_3 into the detector from element e in the target. $N_e(t)$ is the number of scattering centres of element e at depth t in the target. For target atoms at the surface E_3 is given by the kinematical factor k_e :

$E_3 = k_e E$, and in general $E'(E_3) = E_3/k_e$. E_1 is the beam energy *before* scattering for atom e at depth t in the sample. σ is the differential cross-section and $S = dE/dR$ where dR is the average distance travelled by an ion energy E while losing energy dE . The pathlength into the target before scattering is given by x and the pathlength after scattering by x' . P_{in} and P_{out} are respectively the distributions in the projected range along the incoming and outgoing directions.

Of course, the measured spectrum is the sum of the Ψ_e for all the constituent elements of the target. There is usually no way to *measure* individual partial spectra Ψ_e .

Fitting by Simulation: Clearly, to calculate the inverse $N(\Psi)$ is not easy analytically and we describe a new approach to this inverse problem below. The most widespread approach currently is a pragmatic application of trial and error. The standard treatment is to *assume* that the target has a certain structure, to *calculate* the spectrum that would be obtained from such a target, to *compare* with the collected spectrum and then to *iterate* until a reasonable match is obtained. The skilled analyst, from long experience and cunning, recognises certain features of the spectrum and will, usually quite quickly, converge to an acceptable solution.

This approach has a number of major drawbacks. *Firstly*, it is entirely manual, requiring a skilled analyst to give each spectrum a treatment that can easily take hours. (It should be noted that many types of spectra can be treated faster, or require only limited data to be extracted. And of course, analysts have become adept at this.) *Secondly*, large numbers of samples cannot be handled where a full treatment is needed, since the analyst simply runs out of patience. *Thirdly*, because of the difficulty of data analysis the temptation for the experimentalist is to make samples especially for the analysis, instead of analysing the samples that result from the experiment. *Fourthly*, in cases where the experimenter has failed to keep the samples simple, the spectra can be complex so that the analyst has difficulty extracting definite depth profiles from the data: in these cases the analyst may remain uncertain of the validity of the result. *Fifthly*, training these skilled analysts is difficult: they are almost invariably at least postgraduate student level. *Sixthly*, we have developed the "rule of thumb" (rough estimate), over many years of analysis, that to analyse reasonably simple data collected over one day requires three further days subsequent concentrated work by the analyst. Difficult data (or the inexperienced analyst) may take much longer! Clearly, to fully staff an accelerator will be very expensive. There are, currently, few labs offering a full commercial RBS service.

Fitting by Simulated Annealing: We have taken a completely different approach. At its heart is the simulated annealing algorithm, which is a *global* minimisation algorithm using combinatorial optimisation (see the next section). We have applied this algorithm to ion beam analysis (IBA) data, yielding an *algorithmic solution of the IBA inverse problem*. Note that the manual procedure described above is not a true algorithm since it cannot be handled by a machine in the general case. The function of the analyst is now different: instead of trying to guess a rough structure that may be approximately consistent with the data, the analyst concentrates on specifying the machine calibrations, on specifying any prior knowledge of the sample, and on an appropriate metric for the validity of the result. For any given set of priors (these include instrumental parameters) the *algorithm*, not the analyst, will determine the depth profile. We should point out that the algorithm itself, as we have implemented it, has a large number of parameters which could be chosen by the analyst: our implementation has value largely because we have shown that we have found values of general validity for most of these parameters, and we give the analyst clear rules for the choice of the remainder.

We believe that the advent of this new algorithm will completely revolutionise the applicability of IBA techniques to thin film analysis since it addresses each of the six drawbacks enumerated above at a fundamental level. The improvements are so dramatic that we effectively have a new tool for thin film composition analysis.

4- Introduction to Simulated Annealing

In this section we describe the various elements of the simulated annealing algorithm that lies at the heart of the IBA DataFurnace. This discussion is central to this paper.

The essential elements of the simulated annealing algorithm (SA) were invented nearly 50 years ago by Metropolis *et al* (1953) with a group including Edward Teller, in the context of the discussion of the use of "fast computing machines" and Monte Carlo methods to calculate the equilibrium value of any (thermodynamic) quantity using the canonical ensemble of statistical mechanics. They successfully calculated the equation of state for a 2D ensemble with these methods using the Los Alamos MANIAC computer.

The fundamental SA theorem establishes that provided certain formal criteria are observed, the algorithm is guaranteed to find the absolute minimum of any piecewise continuous function. The implementation of the algorithm is always computationally relatively expensive, and a revival of interest in it followed the explosion of computing power in the 1980s. We have found the summary of Aarts & Korst (1989) useful. It has been used to solve previously intractable problems such as, for example, the NP-complete¹ travelling salesman problem (see Press *et al*, 1992), and the construction of automatic sentence parsers for natural language processing (see Wilks *et al*, 1996). It was actually in the context of the last application, serendipitously, that we came across SA. In fact, the NP-complete class of problems has provided an important stimulus for the development of SA, as Kirkpatrick *et al* (1983) point out in an interesting article that uses SA to solve the semiconductor chip layout design problem (as well as the travelling salesman problem).

The Forward Model: We will represent the elemental depth profile of a thin film as a sequence of layers of specified thickness, each containing certain elements in a given proportion. There are other ways of representing profiles, but this is quite general and is the natural representation for the calculation of the expected IBA energy spectra. Consider an arbitrary depth profile \mathbf{x} which is a structure $\{l, \lambda_{ij}\}$, where the vector l is the list of layer thicknesses, and the matrix λ is the list of relative proportions of the elements for each layer (and hence $\sum_j \lambda_{ij} = 1$). Then the *forward model* is encapsulated in the function $F(\mathbf{x})$ which calculates the energy spectrum $\mathbf{Y}(E)$ (cf. eq.1) expected for the sample with depth profile \mathbf{x} .

$$\mathbf{Y}(E) = F(\mathbf{x}) \tag{2a}$$

$$F(\mathbf{x}) = \sum_e f_e(\mathbf{x})$$

where the forward model calculates a *partial spectrum* f_e for each chemical element in the sample, and the total spectrum is just the sum of the partials.

¹"non-deterministic polynomial time complete" - that is, the computation time is not bounded by any power of the number of independent variables of the problem

This forward model, which is discussed in detail later (§8), is the essence of the calculation: without a forward model the spectra cannot be interpreted. All existing simulation programs are essentially simply implementations of the forward model. We consider limitations of the existing forward model at the appropriate place.

The Objective Function: We have to have a way of comparing some profile \mathbf{x} with the measured spectrum \mathbf{Y} . There are many possibilities, some of which we will discuss later. We could use the very simple and general χ^2 function to compare the measured n-channel spectrum $\mathbf{Y}=\{y_1, y_2, \dots, y_n\}$ with the calculated one $F(\mathbf{x}) = \{\psi_1, \psi_2, \dots, \psi_n\}$, given by:

$$\chi^2(\mathbf{Y}, \mathbf{x}) = \sum_i (y_i - \psi_i)^2. \quad (2b)$$

It is not necessary to use the χ^2 function, but some such function must be specified and this is known as the *objective function* $O(\mathbf{Y}, \mathbf{x})$. To solve the inverse RBS problem the objective function has to be minimised. When $O(\mathbf{Y}, \mathbf{x})$ is minimised an *optimal solution* \mathbf{x}_o has been found: $O_{\min} = O(\mathbf{Y}, \mathbf{x}_o)$. Note that there may be many indistinguishable solutions \mathbf{x}_o . Normally we are content with any particular solution \mathbf{x} that is near an optimal solution \mathbf{x}_o , but we show later how to find both a *most probable solution* and also an estimate of the error of this solution.

Markov chains: SA depends on the mathematics of Markov chains (see Gilks & Richardson, 1996). These are simply sequences M_s of states s_i selected from a state space \mathbf{S} such that $M_s=\{s_1, s_2, \dots, s_i, \dots, s_m\}$ where the s_{i+1}^{th} entry in the chain depends only on the s_i^{th} entry and not on any previous ones. More properly,

$$P(s_{i+1} | s_1, s_2, \dots, s_i) = P(s_{i+1} | s_i): \quad (2c)$$

that is, the probability of s_{i+1} given s_i is independent of all states before i .

Then the Markov chain is constructed by the *transition distribution* $T(s_i) = s_{i+1}$. This distribution is composed of a *generation distribution* from which a *proposed* new state is generated, and an *acceptance criterion* which determines whether or not to accept this proposed state as the next entry in the Markov chain.

Barradas, Jeynes & Webb (1997) have pointed out that although \mathbf{S} is extremely large, it is finite in principle because there are only 92 elements, and both sensitivity and energy resolution are finite. As an estimate, for any given beam and detection system

$$\log |\mathbf{S}| \approx (\prod_{i=1}^e 1/\phi_i) \log n \quad (2d)$$

where $|\mathbf{S}|$ is the number of states s in the space \mathbf{S} , there are e elements in the sample, ϕ_i is the relative sensitivity for element i and n is the number of separable layers. Note that typically no more than 50 layers can be distinguished ($n < 50$) and in each layer we can probably not determine the concentration of an element at better than 1% precision ($1/\phi_i < 100$). Therefore the problem may be treated either as a discrete or (since \mathbf{S} is so large) as a continuous problem, depending what is mathematically more convenient.

For SA the Markov chains are constructed in a particular way. The state space \mathbf{S} is the space of all possible depth profiles \mathbf{x} . This is the same as the space of all conceivable samples². The

²In our previous literature we have called \mathbf{S} the "solution space", confusingly since one usually thinks of a "solution" as being the result of the calculation, rather than a step in it.

Markov chains are then sequences of profiles $\{x_1, x_2, \dots, x_m\}$. The generation function for constructing x_{i+1} from x_i can be any method of selecting a new profile x from state space. It is the acceptance criterion that gives SA its remarkable properties.

The Acceptance Criterion: A proposed state x_p is accepted depending on how the objective function has changed from its value for the last element x_i of the current Markov chain under construction. We evaluate the change $\Delta = O(Y, x_p) - O(Y, x_i)$ in the objective function implied by moving from state x_i to x_p , and if it is improving ($\Delta < 0$) we accept the state: $x_{i+1} = x_p$. However, if it is getting worse ($\Delta > 0$) we may *also* accept it according to the probability P given by the *Metropolis criterion*:

$$P \propto \exp -(\Delta / T) \quad (2e),$$

where T is a control parameter characteristic of the Markov chain under construction. It is not hard to recognise the similarity of this probability to the Boltzmann factor, with T analogous to temperature. Thus, for the construction of the Markov chains used in SA the Metropolis criterion (or some generalisation of it) is used for the acceptance criterion: this gives the Markov chains a natural thermodynamic interpretation. If the Markov chains are long enough they will reach a "thermodynamic equilibrium", that is, the expectation value of certain statistics will stabilise. The introduction of a probability into the transition function means that it can be viewed as a Monte Carlo process, and these Markov chain Monte Carlo (MCMC) techniques are currently of enormous mathematical interest (see for example Gilks & Richardson, 1996).

The Cooling Schedule: The final component in SA is the *cooling schedule*. A sequence of Markov chains is constructed with steadily reducing "temperature". Then the SA theorem states that the objective function will be minimised provided that each Markov chain is long enough to have reached equilibrium, and provided that the cooling schedule is sufficiently slow.

Summary: SA is an algorithm for finding the global minimum of an objective function. The entire state space of this function is explored. A sequence of states (a Markov chain) is constructed in which succeeding states have an objective function that is either reducing or has a Boltzmann-like probability of increasing according to a parameter analogous to temperature. Hence the idea of "annealing". A sequence of Markov chains is then constructed with reducing temperature; the end point being an optimal solution. For IBA the objective function for a proposed depth profile is constructed from the difference between the spectrum being fitted and that calculated with a forward model (a standard simulation code) from the proposed depth profile. Then the state space explored is the space of all possible depth profiles.

5- Mixed Metal Silicides

Our first set of examples is in the silicide system. One form of iron disilicide is a semiconductor, and in principle it should be possible to fabricate a heterojunction laser in silicon (Leong *et al*, 1997). On the other hand, cobalt disilicide is a metal, and interesting 3D metallisation schemes seem feasible. Clearly, success with either material is likely to prove revolutionary, but neither is easy to incorporate in the standard silicon process and the Surrey group has systematically explored synthesis by high dose ion implantation.

Analytical Solutions: Nearly ten years ago, in the course of work on ion beam synthesised iron disilicide, we came across a spectrum similar to Fig.1; a high dose, high energy Fe implant into

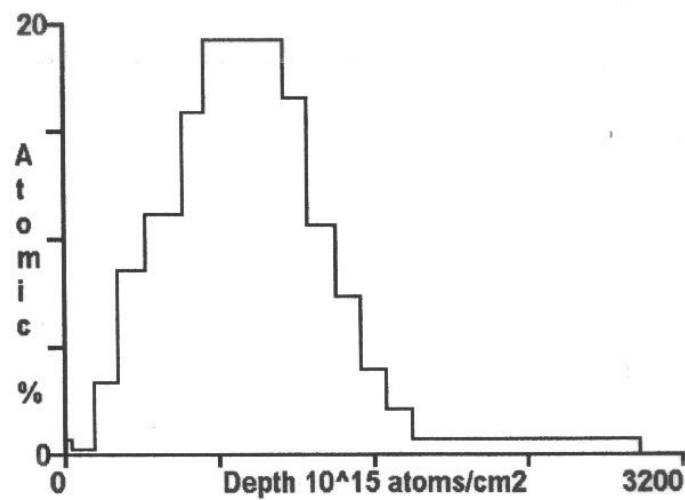
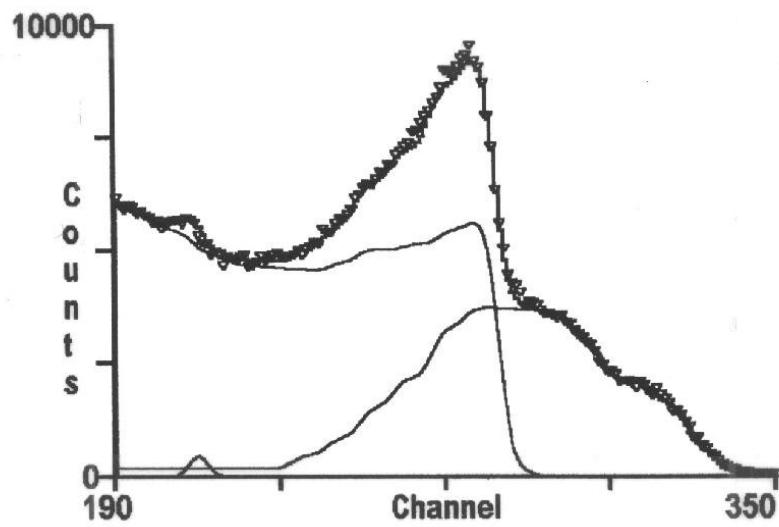
Si such that the Fe and Si signals overlapped. After considerable effort we succeeded in extracting an unambiguous depth profile from the data using the analytical (matrix inversion) code of Børgesen, Behrisch & Scherzer ("SQUEAKIE", 1982). This code reconstructs the depth profile by a closed calculation from the separated partial spectra. Since in this case the partial spectra overlap we used the code iteratively, starting from the surface. (Incidentally, Alkemade *et al*, 1990, use the same iterative procedure.)

In about 1994 a student came to me (CJ) with the spectrum shown in Fig.2, asking for its interpretation. I took some two hours to come to a qualitative solution, but I gave up before I found a very good fit. The student played with the data for many hours, but remained uncertain about the results, subsequently deploying cross-sectional transmission electron microscopy, X-ray photoelectron spectroscopy and other techniques to determine the depth profile (Harry *et al* 1996). The kinematical gap between Fe and Co for these conditions is 18keV, only slightly higher than the system energy resolution of about 15keV (equivalent to about 30nm of Si). Therefore one would not expect there to be much discrimination between Fe and Co. However, as can be seen, there is actually very strong contrast in the spectrum due to the adjacent masses.

Simulated Annealing Solution: After a keen discussion we came to the conclusion that the Børgesen *et al* matrix inversion code could not be used to solve this type of mixed metal silicide problem, and that since in principle it could not be generalised we should look for a different algorithm. To our surprise, it turned out that actually this very contrasty spectrum (lots of strong edges and peaks) is ideally suited to SA: even a rapidly prototyped SA code was able to find a solution very rapidly, taking only minutes on a 100MHz 486 PC. It was clear that SA was a powerful algorithm for solving the inverse RBS problem, and this was the example used for the first report of the "Simulated Annealing of RBS data" (Barradas, Jeynes & Webb, 1997).

Sensitivity to Collected Charge: In Barradas, Jeynes & Harry (1998) the data of Harry *et al* (1996) are re-analysed by SA, this time each fit taking about 2 mins on a 200MHz Pentium PC. Here a PC left running over lunchtime with a batch file of tens of spectra gives results better than those obtained from weeks of labour. The optimisation of the cooling schedule is discussed, together with a demonstration that in this case, with contrast from barely separated masses, the Fe:Co ratio is extremely sensitive to errors in the charge collection. A 1% error in the charge gives a 20% error in the Fe content. Doubtless a careful analytical procedure might increase the precision of this type of measurement, but no-one yet demonstrates charge collection better than 1%. We will return repeatedly to the issue of instrumental parameters and the determination of analytical errors, here we emphasise that the collected charge is a critical parameter in the interpretation of IBA data. This is because for RBS spectra the cross-section is proportional to the square of the atomic number, so the absolute number of counts collected very strongly constrains the possible average Z (atomic number) of the sample. The same applies to all the IBA techniques since they all have strongly Z-dependent cross-sections.

Figure 1: 1.5 MeV ^3He RBS of $2.0 \times 10^{17} \text{Fe/cm}^2$ implanted into Si. a) RBS spectrum with fit (line through data points) and the Fe, Si and O partial fitted spectra (other lines). b) fitted depth profile for Fe. (After Belsen *et al*, 1999).
 Probably the Fe does not penetrate so deeply into the target (there is still apparently "significant" Fe at $2.4 \times 10^{17} \text{atoms/cm}^2$): this is an ambiguity due to uncertainty in the charge collection. There is noticeable surface oxidation in this sample.
 Note on "Thin Film Units" (cf. §8, eq.3): for silicon of density 2.32g/cc or $5.10^{22} \text{atoms/cc}$, one thin film unit ($10^{15} \text{atoms/cm}^2$) is 0.2nm .



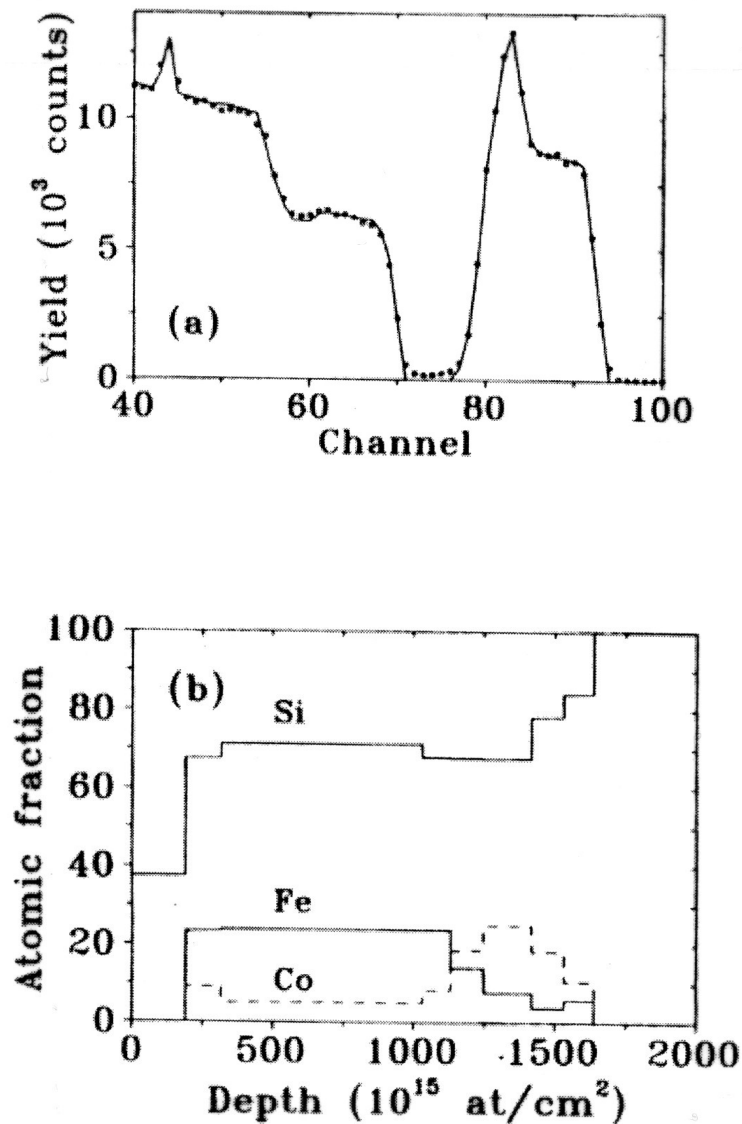
Batch Analysis by SA: In Barradas, Jeynes, Homewood & Milosavljević (1998) examples are shown of data from a set of over 50 samples investigating the kinematics of the ion beam mixing and annealing behaviour of sputtered metal films on silicon (Fig.3). These spectra are also hard, especially since unwanted severe oxidation was experienced in the furnace annealing. By using SA we could rapidly get reliable quantitative data from this large set of hard spectra, which actually allowed us to draw useful conclusions even in the presence of the oxidation (see also Milosavljević *et al*, 2000, 2002). With manual methods we would have had to repeat the experiment.

Fig.3 shows a set of spectra (left hand side) with the corresponding extracted depth profiles (right hand side). The spectral plots show the data and the calculated fits (which go through almost all of the data points), and also the calculated partial spectra. The profiles (right hand side) were obtained using a modified version of the matrix inversion code (SQUEAKIE) of Børgeesen *et al* (1982) which can be applied directly since the partial spectra are available once the SA calculation is complete. The layer structure determined by SA is shown by the histogram lines in the top depth profile (fig.3a, right hand side).

Discontinuity of SA Solutions: This raises the interesting question of which representation is more fundamental, the discontinuous layer structure determined by SA, or the continuous profile determined by subsequently *inverting* the partial spectra calculated by SA? Clearly the real depth profile is continuous, so experimentalists may prefer to see the inversion rather than the raw layer structure. However, the inversion has a number of problems. *Firstly*, the partial spectra are completely dependent on SA. Unavoidable statistical error in the estimation of the layer structure will cascade into the partial spectra and the inverted profiles calculated from them. Moreover the energy loss variation with depth used by the inversion code is a function of the composition, where the layer structure is determined by SA. Therefore the energy loss is an unavoidably discontinuous function of depth. *Secondly*, an iterative process of using the inverted profiles as the basis for a new proposed layer structure is not simple (and maybe not possible) to implement since as the code stands the inverted profiles take no account of the variation of energy resolution with depth (energy straggling). In fact, Børgeesen *et al* specifically point out that their algorithm will not handle energy straggling (or the surface signals) correctly. *Thirdly*, the inversion necessarily assumes the accuracy of the forward model, but errors in the stopping power database (these can be at the 10% level as discussed in detail below) mean that the depths of interfaces may be inconsistently estimated between the different elements in the sample. We have seen very large artefacts demonstrably due to this effect.

We have therefore concluded that the layer structure determined by SA is the more fundamental, and for these and other reasons we no longer use the Børgeesen inversion code. The nominal advantage of the Børgeesen code is that it imposes self consistency on the depth profiles obtained. Since we can demonstrate that these profiles are not internally consistent in general we are better off using a simpler inversion algorithm that does not claim self-consistency. In fact we now use the inversion algorithm common to other simple codes, such as the "profile" command in RUMP (Doolittle, 1986).

Figure 2: 1.5 MeV ^4He RBS of $25 \cdot 10^{16}/\text{cm}^2$ double implants of Co followed by Fe into Si. Implantation temperature was about $350\text{ }^\circ\text{C}$. a) RBS spectrum with fit (solid line) and Co and Fe partial fitted spectra (dashed lines). b) fitted depth profile. (Fig.3 of Barradas, Jeynes & Webb, *Appl.Phys.Lett.* **71**, 1997, 291) The surface is significantly oxidised, but the O profile and partial spectrum are omitted for clarity. The depression in the Si concentration between about 10 and $15 \cdot 10^{17}/\text{cm}^2$ corresponds to a cubic silicide, while below about $10 \cdot 10^{17}/\text{cm}^2$ the layer has a stoichiometry similar to the Si-rich $\alpha\text{-FeSi}_2$ phase.



Occam's Razor: We have up to now invoked the principle of Occam's Razor ("minimise your assumptions"³) in stating that we choose the layer structure with the *fewest* layers to represent the sample. Thus we make the layer structure as coarse as possible consistent with the data (the calculation method is described in Barradas, Jeynes, Jenkin & Marriott, 1998). Note that the quality of fit obtained is outstandingly good even with these very discontinuous solutions. From an analytical point of view it serves to emphasise that we find *an* optimal solution; the solution is *consistent* with the data, leaving open the question of what other different structures may also be consistent with the data, and how different they might be. We return to these questions later, but we note here that it is clear that some sort of continuity condition *ought* to be applied to this type of data and we have not yet satisfactorily determined how such a condition could be specified.

RBS by the Unskilled: Finally, returning to Fig.1, this spectrum was from one of a set of twelve samples created in an experiment set up as an exercise for a group of school-leavers (18 year olds) as part of a national scheme to give this age group a taste for university research. These young people were with us for about ten days in total. In the course of that time they had approximately four hours training in RBS data collection and data reduction techniques. We collected the data for them and set up the analysis but then passed it over to them, and they, essentially unaided, used the DataFurnace software to extract depth profiles from the whole data set, writing up the results (including a full presentation of the methods, aims and complementary optical results) in a single day. This expresses exactly the benefits we believe exist for using this new tool for solving RBS spectra. The data turned out to be very interesting and were subsequently published (Belson *et al*, 1999).

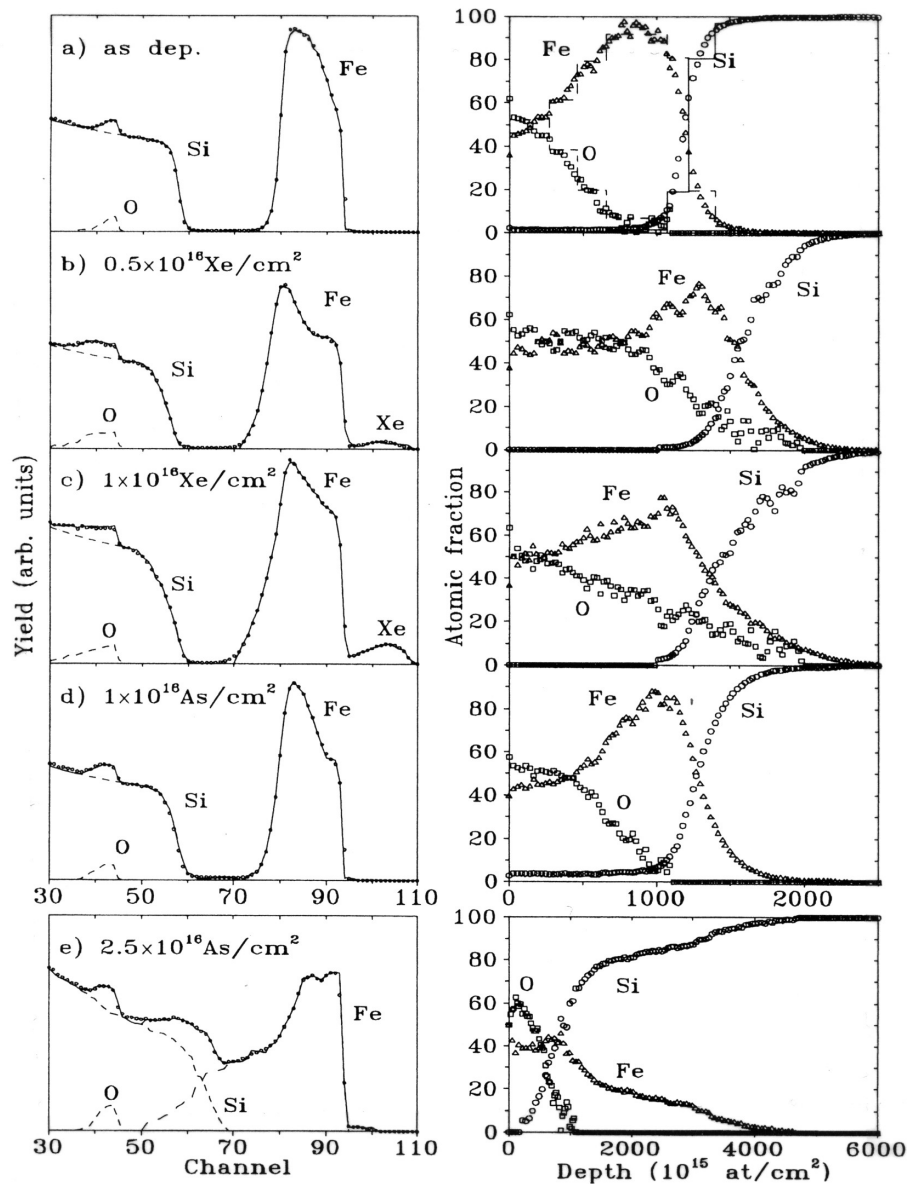
6- Simulated Annealing: Algorithmic Issues

The simulated annealing theorem proves that in the general case a global minimum in the objective function is reached in logarithmic time, that is, for Markov chain k the cooling schedule is given by a temperature sequence $T_k = T_0 / \log(10+k)$, provided that the initial temperature T_0 is sufficiently large (Geman & Geman, 1984). Unfortunately this implies ridiculously long computation times. In practical cases geometrical cooling schedules are always used, that is $T_k = a^k T_0$, where typically in our case $a \sim 1/2$. This implies that SA is efficient for some classes of problem, but may be very inefficient for others.

An interesting paper by Sorkin (1991) has started to show in which circumstances SA can be expected to be efficient. He proves that for a state space with certain (rather artificial) fractal properties, a value of the objective function *close* to a global minimum can be found in geometrical time. But he shows that it is likely that a more general theorem for realistic fractal state spaces is also true. In a preliminary analysis of the state space for a representative RBS spectrum we have found that, in the vicinity of the global minimum and in certain representations (not the χ^2 one described above), the objective function has only one minimum

³William of Ockham, 1285-1347, was known for his extensive use of the principle: *non sunt multiplicanda entia praeter necessitatem* (entities are not to be multiplied except of necessity). See Garrett (1991) for an interesting application of this principle to Bayesian probability. Ockham is now a small village about 5 miles from Guildford.

Figure 3: RBS data with simulated annealing fits (left), and corresponding derived depth profiles (right), of sputter deposited 120nm Fe layers on Si ion beam mixed with either As or Xe and annealed at 900°C for 150mins. In the left column the solid lines are the fitted spectra, and the partial O, Si and Fe spectra are shown as dashed lines. In the right hand column the partial spectra extracted with DataFurnace are replotted as "depth profiles" using SQUEAKIE (Børgesen *et al*, 1982). For clarity, only one fitted depth profile is shown as a histogram (top spectrum, right hand col.). Notice the different depth scale in the right hand column of e). Fig.2 of Barradas, Milosavljević *et al* Nucl. Instr. Methods **B139** (1998) 235-238.



(the global minimum). We therefore suspect that IBA spectra are likely to have quite well behaved objective functions which SA can solve easily. We will report on this in another place.

To demonstrate that our SA algorithm is well behaved we need to show that it converges properly. Barradas, Marriott *et al* (1998) have shown the variation of the average Si content of the last 50 elements (states \mathbf{x}) of each Markov chain in the cooling schedule at various depths for an annealed and oxidised iron silicide (the sample shown in Fig.3e), plotted for the entire cooling schedule. In the substrate the silicon content reaches its final value at a high temperature, but near the surface, where there are many more possible states due to the presence of lots of oxygen (with its small signal and consequent small influence on the χ^2), the final value is not reached until the end of the cooling. Marriott *et al* (1999) have also demonstrated that our MCMC algorithm is well behaved, in particular that it converges and "mixes" properly. Mixing means that the sampling process explores all possible solutions in an efficient manner.

7- The Forward Model

In this section we explicitly state the forward model that we use, and also describe the code structure of the IBA DataFurnace. We also briefly review other simulation and fitting codes.

Simulation: All IBA labs have *simulation codes* to calculate spectra to compare with collected data: these are equivalent to what we have called the *forward model* and have long been available (Brice, 1973). There are a number of codes, with various useful user interface features, which have been well reviewed by Kótai (1994). The DataFurnace is *not* a simulation code; it is a *fitting* code, incorporating a simulation code in its core. It replaces all existing single scattering simulation codes (we discuss multiple scattering codes below in §8). Because the forward model is executed repeatedly for each fit it is optimised for speed. However, some improvement of the algorithm may be obtainable using Serruys' retrograde method (1991).

Fitting: Kótai does not mention Serruys *et al's* interesting "PERM" code (1993) which is a true fitting code based on a novel simulation algorithm (Serruys, 1991) and a novel and efficient spectrum smoothing algorithm (Serruys, 1990). However, Serruys' code is not a true algorithm, relying as it does both on a reasonable initial guess by the user and also on some guidance by the user during execution.

Børgesen *et al's* matrix inversion code ("SQUEAKIE", 1982) is a mathematical attempt to solve the inverse problem which we have already described (§5) and which has severe limitations. A similar but much more general approach has been taken by Kogan *et al* (1994) based on the reduction method for ill-posed problems developed by Pyt'ev (1983). Pyt'ev's method is for linear cases but Kogan *et al* have generalised their treatment for this non-linear problem. Kogan's "Beam Expert" does appear to be truly general purpose, that is, it is capable of inverting spectra where the partial spectra overlap or where there is no unique solution. However, it is also not clear how robust it is to problems of the forward model, in particular those due to errors in the energy loss database. Nor is it clear whether or not it is robust in use, or whether it has instabilities similar to those exhibited by Serruys' code.

Difficulties and shortcomings of this type of inversion code have been comprehensively and elegantly described by Cumpson (1995) for the (related) technique of angle-resolved XPS. Cumpson also compares the properties of inversion and Maximum Entropy algorithms (we describe the MaxEnt code of the Garching group below, §12), and he comments on the

usefulness of the MaxEnt approach, especially when uncertainty estimates are required. Our approach is mathematically closely related to the MaxEnt one..

The RBS Forward Model: The RBS forward model is straightforward to calculate numerically. The sample is divided into thin layers and the scattering of the incident beam (of energy E_0) from each layer is considered. Then the energy of the beam E_q before scattering after crossing layer q is given by an integration of the energy losses on the inward path to the layer:

$$E_q = E_0 - \sec \theta_1 \sum_{i=0}^{q-1} t_i \varepsilon(\mathbf{p}_i, E_i) \quad (3)$$

where θ_1 is the incident beam angle from normal, t_i is the thickness of the i^{th} layer (in thin film units, that is, in $\mu\text{g}/\text{cm}^2$ or equivalent units), and E_0 is the incident beam energy. $\varepsilon(\mathbf{p}_i, E_i)$ is the energy loss (per unit depth, in thin film units) in the i^{th} layer which has a composition given by $\mathbf{p}_i = \{p_{1,i}, \dots, p_{e,i}\}$ where $\sum_{j=1}^e p_{j,i} = 1$ and there are e elements. The number of scattering centres $C_{e,i}$ of element e in layer i is then given by $C_i = t_i \mathbf{p}_i$. Note that this structure $\{t_i, \mathbf{p}_{ij}\}$ has the same chemical elements but a different (larger) number of layers from the depth profile $\mathbf{x} = \{l_i, e_{ij}\}$ defined previously. The layer thicknesses t must be chosen small enough that $\varepsilon(E_{i-1}) \cong \varepsilon(E_i)$ otherwise the numerical integration will cumulate errors.

The energy loss ε is calculated from a database of the energy loss of ions in matter (Ziegler, Biersack & Wittmark, 1985) that extends across the entire periodic table for both beam and target, and for all beam velocities above about that of 50keV H. The energy loss in any target can be calculated by linear superposition of elemental energy losses. Thus

$$\varepsilon(\mathbf{p}_i, E_i) = \sum_{j=1}^e p_{ij} \varepsilon(j, E_i) \quad (4)$$

where $\varepsilon(j, E)$ is the energy loss of the beam energy E in element j . This is known as "Bragg's rule" (Bragg & Kleeman, 1905) and is usually accurate, except near the stopping power maximum for compounds of light elements such as organics, oxides and nitrides, for which deviations as large as 20% have been observed (Rauhala, 1995). The accuracy of the database is limited: errors of 10% can be demonstrated (Niemann *et al*, 1996; Lennard *et al*, 1999).

The scattered beam has an energy D at the detector which depends on the scattering nucleus and the pathlength from the layer back to the surface, and which is calculated with an integral analogous to that of eq.3, but which we will write iteratively for clarity:

$$A_{i-1} = A_i - t_i \varepsilon(A_i) / \cos \theta_2 \quad (5)$$

$$A_q \equiv KE_q; \quad D_q \equiv A_0$$

where the calculation layers i are as before, $\mathbf{D}_q = \{D_{1,q}, \dots, D_{e,q}\}$ is the list of energies at the detector from the q^{th} layer for the e elements in the sample, $\mathbf{K} = \{K_1, \dots, K_e\}$ is the corresponding list of kinematical factors and θ_2 is the exit beam angle from normal. Note that the kinematical factor is the fraction of energy that the incident particle keeps after an elastic collision (so that $\mathbf{D}_0 = \mathbf{K}E_0$), and that this fraction is calculated from conservation of energy and momentum. $A_1 = KE_q$ is the energy at the q^{th} layer after backscattering and the A_i are the energies on the outward path at the i^{th} layer.

The pulse height spectrum is obtained by digitising each pulse from the detector with a multi-

channel analyser (MCA). This spectrum is then transformed to an energy scale by a linear relation (without loss of generality since non-linear electronics can be linearised, see Lennard *et al*, 1990):

$$S_c = \gamma c + o \quad (6)$$

where S_c is the energy represented by the MCA channel number c of the spectrum, γ is the electronic gain (in keV/channel) and o is the electronic offset (in keV) due to the detector pulse height defect. The determination of γ is critical in the system calibration. (Actually, γ is a weak function of c , but this dependence is usually unobservable for surface barrier detectors, see Lennard *et al*, 1990; Jeynes *et al*, 1998).

We now have to transform the layer number of the sample used for the energy loss calculation into the channel number in the spectrum. Note that this transformation is neither linear with depth nor the same for different elements (see eqs.1&2). We calculate the layer number m corresponding to channel number c for e elements of the sample through the inequality

$$D_{e,m+1} < S_c \leq D_{e,m} \quad (7)$$

So that each channel corresponds to a layer at different depth for every element (e values of m for every channel c). Then the beam energy $B_{e,c}$ *before* scattering from element e in the layer corresponding to channel c is given by:

$$\begin{aligned} B_{e,c} &= E_m + r_{e,c} (E_m - E_{m+1}) \\ r_{e,c} &\equiv (D_{e,m} - S_c) / (D_{e,m} - D_{e,m+1}) \end{aligned} \quad (8).$$

Of course, for each element e there is a maximum channel number k (non-integral in general) such that $S_k = K_e E_0$ (where K is the kinematical factor mentioned above). There is also a set of absolute minimum channel numbers z given by $D_z = 0$, although the cutoff energy below which there is no useful information is usually much larger than zero.

The number of scattering centres of element e in the layer m is given by

$$\begin{aligned} N_{e,c} &= C'_{e,c} - C'_{e,c+1} \\ C'_{e,c} &\equiv r_{e,c} C_m + \sum_{i=1}^{m-1} C_i \end{aligned} \quad (9).$$

Note that $\mathbf{B}_e = \{B_{e,1}, \dots, B_{e,c}, \dots, B_{e,v}\}$ is a list of the beam energies *before* scattering where the sample is divided into v layers with each layer corresponding to one *channel* of the spectrum, whereas \mathbf{E} is a list of the beam energies *before* scattering where the sample is divided arbitrarily into equal thickness *calculation* layers.

A partial spectrum for element e of the sample can then be calculated through:

$$f_e = Q\Omega \gamma N_e \sigma'(\mathbf{B}_e) / \varepsilon(\mathbf{p}, \mathbf{B}) \quad (10)$$

where σ' is the differential Rutherford scattering cross-section and the vector notation $f_e = \{f_{e,1}, \dots, f_{e,c}, \dots, f_{e,v}\}$, $N_e = \{N_{e,1}, \dots, N_{e,c}, \dots, N_{e,v}\}$, $\varepsilon(\mathbf{p}, \mathbf{B}) = \{\varepsilon(\mathbf{p}_1, E_1), \dots, \varepsilon(\mathbf{p}_c, E_c), \dots, \varepsilon(\mathbf{p}_v, E_v)\}$ are used as before, with v relevant channels in the spectrum for element e .

The product of the collected charge and detector solid angle $Q\Omega$ is another critical calibration

parameter.

The complete spectrum is then given by the summation of all the constituent elemental spectra:

$$\mathbf{F} = \sum_e \mathbf{f}_e \quad (11)$$

and the detector resolution is convoluted into \mathbf{F} if required. Energy straggling (or, more generally, the depth dependent energy resolution) is convoluted into \mathbf{f}_e if required, but this significantly increases the computation time, and therefore is only used where necessary.

Forward Model changes for other IBA: For EBS we simply substitute a different (numerical rather than analytical) scattering cross-section function for σ . The ERD forward model is almost exactly the same except that the recoil rather than the scattered particle is followed on the outward path. Also we permit a range foil before the detector (for either RBS or ERD: it only requires extra energy loss on the outward path). Time of flight ERD (ToF-ERD) does not require any modification of the algorithm: it requires only being able to handle multiple spectra: for this technique the 3D data set can be separated into a series of spectra, generally one for each element. Heavy ion ERD (HI-ERD) requires no modifications: the interaction cross-sections are generally Rutherford and the stopping cross-sections are tabulated in the semi-empirical database. HI-ERD is usually carried out at a recoil angle sufficiently large for the high intensity forward scattered primary beam to be kinematically prohibited. Where this condition is not satisfied some other means must be found to exclude this beam: ToF techniques can work for a low intensity or a pulsed primary beam, or a range foil can be used with a surface barrier detector. In the latter case the different recoil ions may be superimposed in the same spectrum and cannot be separated by the detector. In any case the DataFurnace can handle the data.

For NRA the situation is somewhat different. The model outlined above for RBS assumes implicitly that there is a monotonic relationship between depth and channel number for any particular elemental signal. This is not always true for NRA, and DataFurnace (Barradas & Smith, 1999) use a different (more cumbersome) algorithm that takes this into account, unlike other NRA codes (Lennard *et al*, 1993 also gives a correct treatment). Otherwise, for NRA we only have to modify the kinematics formulae to allow for the non-zero Q values, introduce the appropriate interaction cross-section values (as for EBS), and specify and follow the appropriate detected particle (as for ERD).

PIXE: DataFurnace does not support PIXE. The PIXE forward model is entirely different in structure from the particle scattering models, and it is not trivial to modularise existing codes, such as GeoPIXE (Ryan *et al* 2002) or GUPIX (see Blaauw, 2002) for use in SA. There is not much depth sensitivity in PIXE data, just as there is often considerable ambiguity about mass in RBS, so these two techniques are highly complementary. Geoff Grime (1995) has provided a powerful user interface to give GUPIX users effective simultaneous access to RBS.

The IBA DataFurnace: Simulated annealing is a *modular* algorithm involving four modules: the forward model, the generation function, the acceptance criterion and the cooling schedule. Different functions can be substituted for any of these four modules without changing the fundamental operation of SA. Therefore we can use different forward models with essentially no change in the code.

The DataFurnace is a hybrid code, with a preparation algorithm that characterises the spectra and determines parameters for the SA cooling schedule, the simulated annealing algorithm itself,

and a final local minimisation routine that takes over at low temperatures. This latter is because although SA is a very efficient global minimisation algorithm it is very inefficient at determining true local minima.

The preparation algorithm uses an adaptive filter to very effectively smooth the spectrum without significantly changing the position or width of peaks and edges, and then it counts peaks and edges. The local minimisation routine is a grid search routine which is very stable (although rather slow) in high dimensional spaces (common in DataFurnace analyses).

8- Forward Model limitations: multiple scattering

RBS of O Implants into SiC: We have recently been successful in making waveguides in SiC by implantation with the lowest reported losses so far (Vonsovici *et al*, 1999). We used high dose high energy ion beam synthesis O implants to form a buried oxide layer. Figure 4a shows an example of the RBS spectrum from one such sample. This is very clearly a good example of a "hard" RBS spectrum since the C and O signals overlap and the profile shape is arbitrary - we know for example that the O profile is not the implanted "Gaussian" shape that can be calculated. The student who broke the ground in this project had dozens of these spectra to analyse, since there was a large matrix of implantation and annealing temperatures to explore (Jackson, 1998). Again, it turned out that SA readily solved these spectra, making RBS a useful tool for the project yielding extremely valuable quantitative results. For the sample illustrated in fig.4 a continuous buried SiO₂ layer has not formed: this occurs at higher implantation temperature.

Low energy effects: The interesting thing here is that the signal comes from deep in the sample with the information being carried by very low energy backscattered particles. In these conditions our RBS forward model is inaccurate, assuming only single collisions, where actually there is a significant low energy signal coming from multiple and plural scattering. (Multiple scattering involves many small angle scattering events and plural scattering involves multiple large angle events.) These effects are well understood: Rutherford had already made reasonable estimates of multiple scattering in 1911, and accurate Monte Carlo calculations can now be made (Bauer, Steinbauer & Biersack, 1992 & 1993).

However, the forward model is core code in SA, executed for each trial x from the state space, and therefore implementing a correction in MC code is out of the question, due to the computational time involved. Mayer (1997) has given a partial solution to this problem with his SIMNRA code which implements a "dual scattering" calculation which is able to account for much of the low energy background observed. Eckstein & Mayer (1999) give an illuminating discussion of how good the SIMNRA approximation is (it is surprisingly good!). The spectral broadening introduced by multiple scattering is calculated correctly in Szilágyi's DEPTH code (see below in "High Depth Resolution" §13).

DataFurnace correction: We here describe our *ad hoc* solution to this problem (Barradas, Jeynes & Jackson, 1998), and discuss its effects. These *multiple scattering* effects cause the yield to increase at low energy. Since the increase is expected to be quadratic in the forward model (since the RBS cross-section goes inversely as the square of the beam energy) we take a faster dependence than this to be cubic as a first order approximation. We therefore compare a spectrum from unimplanted SiC with a simulated spectrum (the spectrum calculated with the forward model), and determine the cubic function that transforms one to the other. We then

incorporate this function into the forward model for the *Si* signal, since it is a correction which applies deep in the sample, and the *Si* signal comes from the deepest regions. It turns out that this correction is analytically very satisfactory since it applies equally well to the spectra from the implanted samples.

Although we expect multiple scattering to modify the forward model, it should be emphasised that our correction is entirely *ad hoc*. We have simply introduced several extra fitting parameters to get a better match with the low energy part of the spectrum. Therefore we will refer to the "MS correction", and point out that it is a background subtraction device rather than a solid analytical calculation.

Good fitting: Is such a device of any real value? The answer is yes, for interesting reasons. SA depends on the objective function being sensitive to moves in state space away from the optimal solution \mathbf{x}_0 . As mentioned in Barradas, Jeynes & Webb (1997), we normalise the objective function $\Delta(\mathbf{x})$ such that $\Delta(\mathbf{x}_0) \approx 1$. So if an error in the forward model means that $\Delta(\mathbf{x}_0) > 1$ we increase the size of the set of near-optimal solutions for any given value of $\Delta > 1$. In other words, to get a *precise* solution (one that discriminates reliably between similar structures) it is necessary to have a good fit.

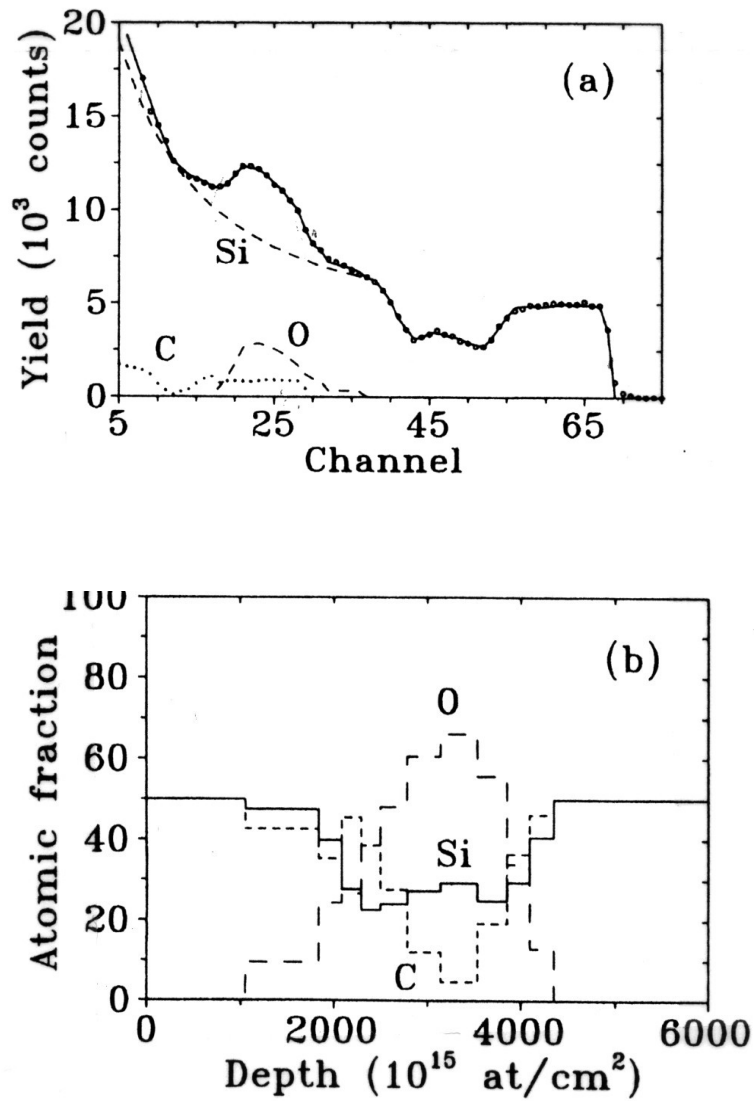
Therefore, for a reliable interpretation of the *difference* between similar complex spectra like that in Fig.4 we must introduce the MS correction. The question then is, how *accurate* is the result? We explore this question in detail later, but in this case we note that the correction is applied to the deep part of the *Si* signal, is small at the depth of interest, and is analytically robust (it can be transferred from the unimplanted sample to the other implanted samples).

There are a variety of artefacts that can give rise to extra (or reduced) low energy signal, including incorrect beam handling, error in the nominal backscattering angle and electronic faults. With the use of the MS correction these will affect the accuracy but not the precision of the SA calculation.

9- Ambiguity in IBA data: Multiple Spectra

Previous Work: Every analyst has tilted the sample and taken another spectrum to determine which features of the spectrum come from the surface: the *surface* signal position does not vary with beam angle, although signals from below the surface will appear to move as the geometry changes. An equivalent way of doing this is to use two detectors at different scattering angles. Of course, this is not a new idea: Williams and Möller were using two (or more) detectors in 1978 (although with a rather different purpose) and Edge (1988) showed calculations emphasising the value of spectra from two detectors, but using an iterative method of calculation not easy to extend to three or more spectra and that we rejected when we were considering incorporating the matrix inversion code (Børgesen *et al*, 1982) into a general algorithm. Butler (1990) emphasises the value of multiple detectors and Alkemade *et al* (1990) have demonstrated that for a sample with n elements, one needs to collect $n-1$ different spectra to eliminate ambiguity in principle. However, with manual methods the analyst has to laboriously fit each spectrum in turn: this is a very large disincentive to collecting multiple data, or, even if they are collected, to analyse them (although many simulation codes give assistance with this.)

Figure 4: a) RBS spectrum (dots) of SiC implanted with $200\text{keV } 14.10^{17}\text{O}/\text{cm}^2$ at 180°C together with the simulated annealing fit to the data (line). The partial Si, O and C spectra are also shown. b) Depth profile determined by SA. Fig.2 of Barradas, Jeynes & Jackson, Nucl. Instr. Methods **B136-138** (1998) 1168-1171



Simulated Annealing: SA uses a different approach: instead of asking for a spectral inversion procedure that finds the unique solution (assuming that there is sufficient information), it uses a procedure that finds any solution consistent with the data. Therefore, even if the data are ambiguous a solution can be found and the algorithm will not crash. We should emphasise that no machine methods for self-consistently inverting *multiple* spectra have been presented, apart from SA.

Because SA is minimising an objective function, and since we can use a different objective function for each beam geometry, it is simple for SA to calculate a composite objective function for multiple spectra. This composite function is described in Barradas, Jeynes, Webb, Kreissig & Grötzschel (1999): briefly, we give each spectrum in the set equal weight irrespective of the integrated counts in the spectrum. We emphasise that SA will do its best to find a solution consistent with *all* the data. The computation time is affected for multiple data sets since as many simulations have to be calculated from different forward models as there are different spectra. However, the calculation is highly modularised and optimised for speed, and having calculated one forward model the others are much less tedious. Also the cooling schedule is faster for multiple spectra since we expect the minima in state space to be better defined. For both of these reasons computation time increases less than linearly with the number of spectra.

Although implementing SA of multiple data sets is nearly trivial, the resulting power made available to the analyst is enormous. Multiple detectors, or geometries, or beams, or even techniques can be used, with no penalty to the analyst in data analysis time after the calibrations have been established. We will give examples of all of these. In particular, a self-consistent analysis is very valuable in accurate work where demonstrably independent confirmation is a prime requirement to validate the measurement. Instead of repeating the analysis we only have to collect double detector data and show self consistency

Example - RBS of B in Si: As an example of this we have considered a nominally BCN film deposited on Si by magnetron sputtering (Barradas, Jeynes, Kusano *et al*, 1999). These films are of interest because of a predicted hardness, stiffness and conductivity comparable to diamond. The determination of composition is actually quite difficult: it is hard (or impossible) to resolve the light elements by electron probe microanalysis (EPMA), even if a windowless X-ray detector is available, and e-beam induced X-ray measurements are troublesome to interpret for these very thin films. RBS, on the other hand, is not very sensitive to low Z elements, especially on a high Z substrate. However, we have shown that a self-consistent analysis of multiple spectra can be used to confidently extract and quantify very small signals. For this sample two beam energies were used, with random and channelled spectra being collected for each. The channelled spectra gave much better signal to noise ratios for the light elements: the MS correction was used for all spectra to fit the Si background signals. In this case the film composition was {B, C, N, O, F} = {15.6(2.1), 7.0(3.1), 30.9(0.9), 37.7(0.6), 8.8(0.4)} where the (1 sigma) statistical error is given in brackets. The detection limit for B in this analysis was 7at% (99% confidence).

Example - Spectra with large dynamic range: This is a rather different example. Often samples are analysed which have (relatively) heavy element minor constituents with a light element matrix. Thus, Mallégol *et al* (2002) have analysed surface treatments of latex films where the interest is in the distribution near the surface of elements characteristic of surfactants. These spectra have to be displayed on a log scale, and a simple use of DataFurnace results in the

minor elements being simply ignored since the number of counts are not sufficient to affect the χ^2 sum by much. In this case we can split the spectrum into two (or more) parts, and combine the χ^2 for the separate parts in the same way that we did for separate spectra. Then a good fit is obtained for the whole spectrum. The only problem to mention is that DataFurnace must not be allowed to change calibration constants (including charge) independently for these split spectra.

10- Ambiguity in IBA data: Restricting the State Space

Mixed silicide example: It is very easy to demonstrate that RBS spectra are ambiguous: the mixed silicide sample of Fig.2 could have metal deep in the sample for example, as discussed in Barradas, Jeynes, Jenkin & Marriott (1999) (BJJM99). Butler (1990) has shown an example which is ambiguous in the sense that different depth profiles exist where different partial spectra add up to the same total spectrum: we discuss this interesting case below. However, we have not (yet) found any examples where IBA data are systematically ambiguous in the sense that the system is "frustrated" in Kirkpatrick *et al's* (1983) terminology; that is, where a large number of optimal solutions exist between which are large potential barriers.

When interpreting such data as the mixed silicides described above (Fig.2) analysts are used to ruling out the possibility of metal deep in the sample because they know that in this case the substrate is pure silicon. However, we have demonstrated that the *most probable* solution of this *spectrum*, assuming that there is *no* prior information, is that there is some 5at% metal in the substrate (BJJM99). It is important to be objective about what we know about the sample *a priori*. If we assume *nothing* about the sample then we have to give a range of possible solutions, consistent with the data. We did this crudely using the MCMC code to simply specify an "error bar" on the calculated depth profile. The median solution has substantial metal and over 50at% O for the substrate. The MCMC code determines the most probable solution, and explores state space around it, effectively determining the *density of states* in state space. Because we only calculate the variance of this distribution of states we will clearly not recognise bimodal, skew or any other non-normal distributions. Of course, much more sophisticated statistics are available from an MCMC treatment.

Interestingly, we also used this mixed silicide example to demonstrate that provided the state space is suitably restricted the RBS data are remarkably *unambiguous* with respect to collected charge (total number of counts). It is common for analysts to collect large amounts of charge to get "smooth" data, but very small charges (we show 0.1 μ C with 2.5msr detector solid angle, BJJM99) can give objectively quite well-determined solutions even for this "hard" case, with the right number of layers and qualitatively the right stoichiometry in the layers. Of course, with less counts in the spectrum the statistical errors on the stoichiometry and layer thickness increase as expected.

This example makes it very clear that the spectra are grossly ambiguous in principle, and we have to give the analyst tools for *excluding* regions of the state space which have a high density of false solutions. The solution we want, with a pure silicon substrate, is a perfectly good solution. However, it is unique; a singular solution, and to find it we have to *explicitly* exclude the "infinite" number of solutions involving impure substrate. This is easily done in practice by specifying the depth and concentration range for one or more of the elements, and constructing the generation function appropriately. It is possible to *overspecify* the state space restrictions so that the code cannot find any solution: in this case the code will give a warning, and the

"solution" found will not fit the data! Actually, for Fig.2 the only restriction required is for the O to be limited to the near-surface region.

Mixed oxide example: Butler (1990) takes a different approach with an example of an oxidised NiCrAl alloy that we show in Fig.5. He points out that for this example the false solutions can be eliminated if prior *chemical* information is taken into account. Thus, he knows that the oxygen comes from the oxidising process, and therefore enters through the surface. (Actually, most of his false solutions are eliminated simply by excluding O from the substrate.) Moreover, the O binds with the metals in well known ways. In his simulation code he gives the analyst tools to manipulate *molecular* (rather than atomic) depth profiles.

We do the same thing by allowing the analyst to specify *molecules* rather than (or as well as) atoms. Fig.5a shows the elemental depth profile of Butler's example with a spectrum calculated from it (Fig.5b). We then ask DataFurnace to invert this spectrum to retrieve the profile under a variety of assumptions. Fig.5c shows the closest DataFurnace could get to the original profile, and we discuss this result further below. We point out here that the result is essentially identical to the original, except for some interface broadening (we have not deconvoluted the straggle).

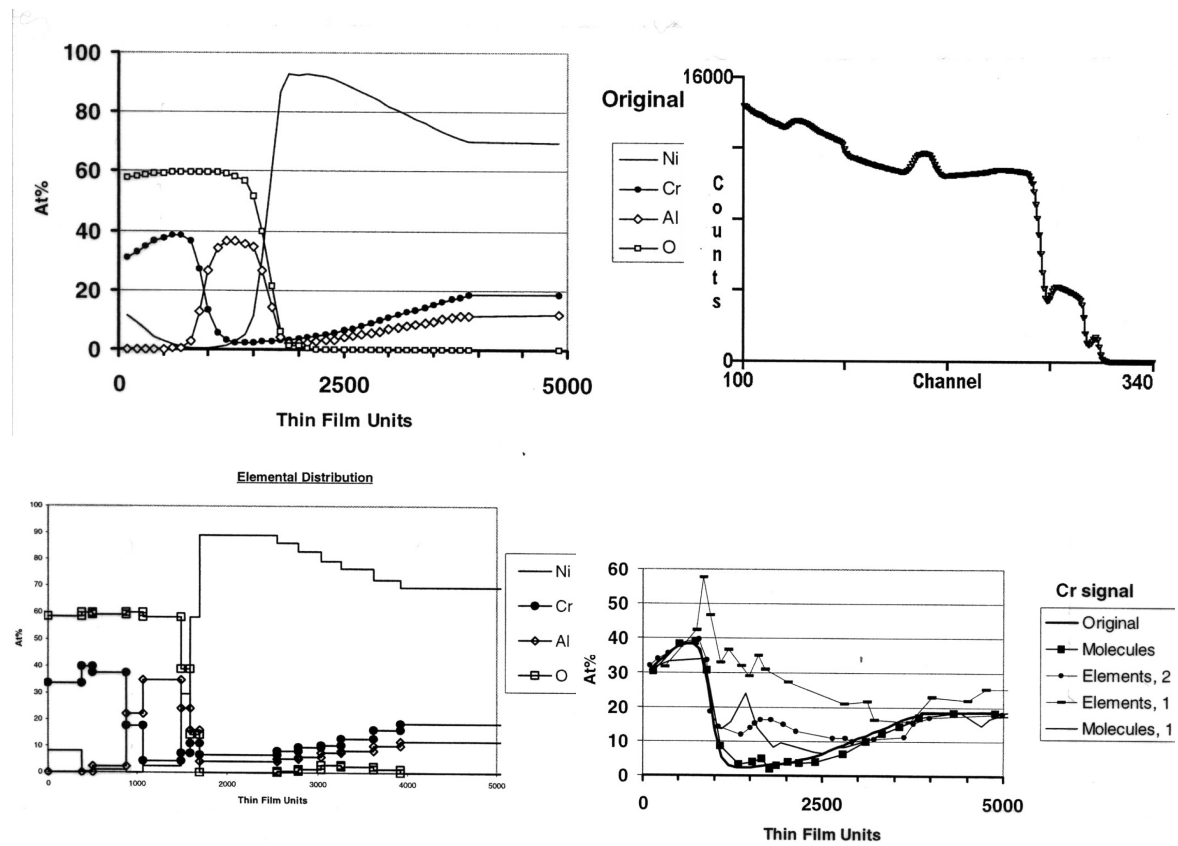
It turns out that the Cr profile is the most sensitive to the prior assumptions of the analysis, and Fig.5d shows the Cr profiles obtained by DataFurnace under four different assumptions. To retrieve Butler's initial profile unambiguously we need to specify not only the molecules present but also that *only* oxides are present near the surface *and* that oxygen is excluded from the substrate *and* that Al is excluded from the near surface region *and* that two independent spectra are taken (at different scattering angles in our example). Butler did not point out this last condition for this example, although he noted that, in general, multiple spectra are always a help. These particular data are very ambiguous: excellent fits can be obtained without any of the conditions mentioned, and they are all as good as that shown in Fig.5a.

In this example we have only allowed the O to exist bound to metals, and we have only allowed free Ni to exist. The substrate is specified by a molecule representing the starting alloy composition. Of course, DataFurnace does not require the analyst to input anything else: the fit proceeds automatically as soon as the initial assumptions are stated. The interesting thing is that it is very easy to specify various assumptions about the chemistry to see whether they are consistent with the data. If they are *not* consistent they can be ruled out. Now the analyst has an effective tool not just for obtaining *a* solution to a spectrum, but for testing a variety of assumptions about the sample against the data.

We must emphasise that we can only extract information from a spectrum if the information is really there. DataFurnace cannot extract more information than exists! But DataFurnace can be used as a tool to explore the validity of various prior assumptions about the sample. It can also be used as a tool to explore what further information would be useful to reduce ambiguity.

Polymer Example: Ross *et al* (2001) have used RBS in conjunction with XPS and other surface specific techniques to investigate the alkaline treatment of poly(vinylidene fluoride) samples in the presence of phase transfer catalysts. This is a very difficult analysis since the spectra are relatively featureless and is thoroughly ambiguous in the absence of any chemical information in much the same way as Butler's mixed metal oxide example above. However, the analysis is successful when the chemical state of the various elements is specified. The defluorination kinetics was shown to follow the Fickian diffusion law with a treatment depth of over a micron.

Figure 5: Re-analysis by DataFurnace of the data shown by Butler (1990) of an oxidised NiCrAl alloy. **a)** the original profile from which the spectrum was calculated; **b)** spectrum (symbols) and fit (line); **c)** atomic profile fitted to data assuming molecules and complete oxidation from the surface, using two spectra at different detector angles, and excluding alumina from the surface; **d)** a comparison with the original profile of the Cr profile calculated under various assumptions. Specifying only elements barely constrains the profile, and even with two detectors the profile is not recovered at intermediate depths. Using only one detector with the assumption of molecules is also not sufficient. Molecules used are NiO, Cr₂O₃ and Al₂O₃.



Interestingly, to complete this work a large batch of several dozen samples had to be analysed.

11- Examples of ERD

DataFurnace can accept a wide variety of analytical conditions. ERD is interesting since it is used in widely different ways in different labs. Barradas, Jeynes, Webb, Kreissig & Grötzschel (1999) analysed a silicon oxyfluoride film using 35MeV Cl^{5+} with two separate beam geometries and three different detectors including a silicon surface barrier detector with a range foil specifically for recoiled H, a Bragg detector and a ToF (time of flight) detector. The latter two detectors have similar signals but different surface sensitivities. It is interesting that DataFurnace can easily cope with the signal overlaps that are so inconvenient for manual analysis in all of these detectors in the same way that it does for RBS spectra. Of course, the practical difficulty with this sort of analysis is that one is often overwhelmed with information. In this example there are ten different spectra available, each carrying different information. All ten were fitted simultaneously with the DataFurnace, which also weights them according to their sensitivities in a completely objective way. This is also a good example of multiple analyses being done with a variety of techniques, detectors in this case. The data is very easy to collect, and now, with the DataFurnace, it has become very easy to analyse.

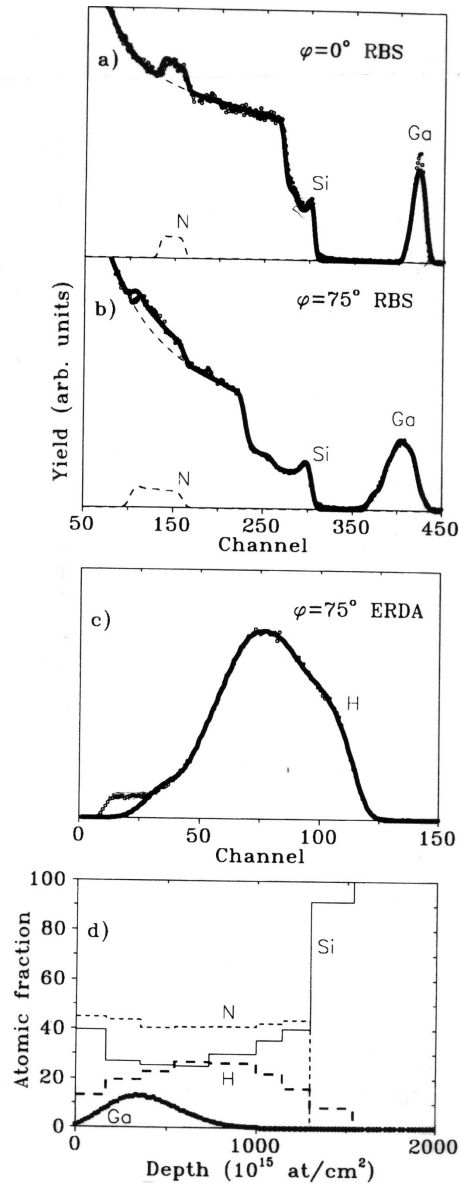
It is also possible to do very satisfactory H determination using ERD with a 1.5MeV $^4\text{He}^+$ beam and a 6 μm mylar foil to range out the forward scattered ^4He primary beam. A good example is shown in Fig.6 (Barradas, Almeida *et al*, 1999), where we were trying to synthesise an amorphous GaN by implanting an amorphous hydrogenated silicon nitride with Ga. Crystalline GaN is an exciting material for blue LEDs, for example, but it is believed that the *amorphous* material could also be very interesting, perhaps for applications like large area displays.

However it is hard to make GaN, and ion beam synthesis was an interesting possibility. The question following the implantation is, does the Ga substitute for the Si or the N? The RBS on its own is equivocal in the presence of so much hydrogen, but with the clear H signal obtained with the ERD (showing H loss near the surface due to the implant) an accurate profile calculation can be made using the right function of energy loss with depth. This data suggests that in this case the Ga is substituting for Si, implying the presence of GaN. We consider the precision of this result in the next section. GaN bonding has been demonstrated by XPS (Almeida, Silva, Sealy & Watts, 1999). It turns out that this only occurs where the a-SiN_x has excess nitrogen.

12- Precise IBA: Quantifying the Error by Bayesian Techniques

In the example of the ion beam synthesised GaN above (Fig.6) we extracted a depth profile that showed a negative correlation between the implanted Ga and the Si concentration. As it stands the result is only suggestive because it is not clear, and it certainly has not been demonstrated, that profiles for which this negative correlation does *not* exist are *excluded* by the data. The given profile is demonstrably consistent with the data but other qualitatively different profiles have *not* been shown *inconsistent* with the data. Clearly, one could play with the profiles and a simulation code and convince oneself that a different conclusion is excluded, but to convince a sceptical observer a more systematic approach is required. In this section we will show that our MCMC methods can easily be applied to estimate the likelihood of a particular profile, given the data.

Figure 6: RBS/ERD of PECVD a-SiN_x:H implanted with 75keV 75.10¹⁵Ga/cm² and annealed in N₂ for 30 mins at 200⁰C. a) RBS, normal incidence. b&c) RBS and ERD respectively, collected simultaneously with backscattering angle 150⁰, recoil angle 26⁰, beam incidence angle 75⁰. The solid lines are the fits; N partial spectra are shown. d) Fitted depth profile. Fig.3 of Barradas, Almeida et al, Nucl. Instr. Methods B148 (1999) 463-467. Also see Fig.8.



Previous Work: Various workers have addressed this problem in different ways. Doolittle (1986) noted that the local minimisation technique in his popular program "RUMP" yielded a Hessian matrix whose covariance represents the uncertainty. However, the minimisation provided by RUMP is rather unstable and in any case depends on the user to get a solution which is nearly correct. Børgeesen *et al*'s (1982) matrix inversion code also yield uncertainties naturally but these are not implemented in the distributed ("SQUEAKIE") code, which in any case requires the user to separate the elemental signals, as we have noted above.

MaxEnt: Fischer and co-workers (1997, 1998) have approached the problem from a completely different angle. They have used Bayesian statistics, with a maximum entropy prior, to deconvolute the detector resolution from RBS spectra of a Co thin film, improving the real depth resolution by nearly an order of magnitude, and resolving the signals from the isotopes of Co.

Unfortunately this astonishing feat involves not only heavy computation but also detailed knowledge of the detector transfer function (the detector resolution, which is a function of both time and detected energy). The group (following our work) used the same methods to extract depth profiles from RBS spectra of thicker films (Prozesky *et al*, 1999), and they have also demonstrated reliable background subtraction for PIXE spectra (Padayachee *et al*, 1999) and even extracted some depth information from PIXE data (Prozesky *et al*, 1997). Of course, the precision of a result is yielded intrinsically by this method.

Maximum likelihood techniques have been used by Liew *et al* (1994) to extract depth profiles from PIXE spectra. Rokita *et al* (1997) have also used maximum entropy to improve the spacial resolution of microbeam PIXE maps.

Simulated Annealing: We can understand Fischer *et al*'s maximum entropy calculation to be analogous to a Fourier transform of state space: it is carried out in reciprocal space, to use an analogy from crystallography. This is because it is natural to work in Fourier space when a convolution function (the detector resolution function) is central to the problem. Our simulated annealing calculation, on the other hand, is carried out in real space: state space is explored with a series of real depth profiles x_i . Because we do not work in reciprocal space we have at least an order of magnitude less computation. However, uncertainty information is yielded equally naturally by our SA formalism.

We wish to quantitatively evaluate the precision of the determination of any given profile. Looked at another way, we wish to determine the size of the set of near-optimal solutions, which we can denote by $\{x_{0+\delta}\}$, with objective function $O(x_{0+\delta}) = O(x_0) + \delta$ for any given value of δ . How much can we perturb the solution we have obtained, and still get an acceptable result? Of course, from a Bayesian point of view all states x are assigned a probability, with the states x_0 having the highest probability. In SA we construct a sequence of Markov chains with reducing "temperature", but we choose the cooling schedule such that as soon as each Markov chain is long enough to be near to equilibrium we reduce the temperature and start constructing the next Markov chain. If, instead of doing this, we construct a *long* Markov chain and ignore the initial non-equilibrium part, what we have is a set of states selected randomly from state space according to the probability given by the density of states.

Bayes Theorem: This can be treated formally with Bayesian methods (cf. Barradas, Jeynes, Jenkin & Marriott, 1999). Because of the existence of measurement error (including statistical

noise and uncertainty in the experimental parameters), the observed spectrum \mathbf{Y} can be treated as a probability density function $p(\mathbf{Y}|\mathbf{x})$ ("the probability of \mathbf{Y} given \mathbf{x} "), which can be calculated simply by using the forward model together with Poisson statistics (although we are not restricted to a Poisson distribution). Then if we can sample from $p(\mathbf{x}|\mathbf{Y})$, the probability density function for the depth profile \mathbf{x} given the observed spectrum \mathbf{Y} , we can also calculate the mean solution $\langle \mathbf{x} \rangle$ and the standard deviation $\sigma(\mathbf{x})$. But Bayes' theorem (1763; for an introduction to Bayesian methods see Lee, 1997) states:

$$p(\mathbf{x}|\mathbf{Y}) = p(\mathbf{Y}|\mathbf{x})p(\mathbf{x})/p(\mathbf{Y}) \quad (8)$$

where the *prior distribution*, $p(\mathbf{x})$, represents any knowledge we have of the sample before we do the analysis. $p(\mathbf{Y})$ is independent of \mathbf{x} and is treated as a constant of proportionality. Then the general theory of Markov chains (see for example Gilks & Richardson, 1996) tells us that the *posterior distribution*, $p(\mathbf{x}|\mathbf{Y})$, is given by the equilibrium distribution of a Markov chain constructed with a Metropolis criterion.

Error Calculation: In order to calculate the confidence interval of any particular solution, and hence find all the plausible solutions, we run a Markov chain based on sampling from $p(\mathbf{x}|\mathbf{Y})$ and use this sample to calculate the simple statistics $\langle \mathbf{x} \rangle$ and $\sigma(\mathbf{x})$. In practice it is sensible to start this chain at a solution \mathbf{x}_{SA} obtained from simulated annealing, and let it run long enough to get reliable estimates of the moments. There are very strong links between the Markov chain Monte Carlo (MCMC) algorithms required by the Bayesian approach and SA, the main difference being that the MCMC algorithm stores a large set of plausible solutions calculated during a run rather than simply the final state stored by SA. This is an extra overhead with a penalty in the computation time, but the advantage is that both the average solution $\langle \mathbf{x} \rangle$ and the most probable solution \mathbf{x}_{mp} are determined, together with a reliability estimate $\sigma(\mathbf{x})$. Note that in general $\mathbf{x}_{SA} \neq \langle \mathbf{x} \rangle$ (and also $\mathbf{x}_{SA} \neq \mathbf{x}_{mp}$) and therefore the Markov chain is run for a "burn-in" period of a few thousand proposals before calculating moments.

From the set $\{\mathbf{x}_{0+\delta}\}$ of possible solutions it is possible to calculate confidence intervals for the structure of the sample. The information in these confidence intervals can be *insightful* for the analyst as is shown by the following simple example of the mixed metal silicides discussed with Fig.2 above.

Consider estimating the total amount of each element up to a given depth in the sample. Both algorithms will give estimates of such a quantity, with the MCMC algorithm being able to also calculate the standard error of these estimates. Such standard errors can tell the analyst much about the quality of the information in a spectrum.

Fig.7 shows data from an MCMC analysis of a mixed metal (Fe and Co) silicide spectrum (these data were actually derived from the spectrum shown in Fig.2 of Barradas, Jeynes & Webb, 1997; this is similar to our Fig.2 above). Fig.7a shows a plot of the set of estimates of the total amount of Fe compared to the corresponding estimate of the total amount of Si. This set of solutions clusters around the SA solution (showed by the solid lines). The spread of the set shows the degree of uncertainty in the solution. For example the SA estimate for the amount of Fe is 262.10^{15} atoms/cm², while the MCMC calculates the standard error of this as being 1.7%.

This analysis can do more than simply calculate standard errors, useful as that is. Fig.7b show the result for Fe and Co. Note the much higher negative correlation in this plot compared to the

left hand plot. What this is showing the analyst is that the information in the spectrum about the amount of Si is reasonably independent of the information on the amount of Fe (since the contours are nearly circular in Fig.7a): however there is very strong dependence in the information about the two metals in the sample. This analysis shows clearly that the spectrum gives a very precise estimate about the total amount of metal but is much less informative about the exact proportions of each. Such ambiguity could be resolved by adding molecular assumptions to the analysis. We will report elsewhere on the further development of general mathematical tools based on MCMC for investigating intrinsic spectral ambiguity (Marriott *et al*, 2002).

We have applied a simple MCMC implementation to the GaN:H data of Fig.6 and obtained the result shown in Fig.8. For each element the lines show \pm one standard deviation from the expectation value of the depth profile. This is a direct representation of the analysis precision. The conclusion that was *suggested* by the SA result is *confirmed* by the MCMC calculation.

13- High Resolution RBS: A Proper Treatment of SiGe Multilayers

Energy Resolution at Glancing Incidence: Analysts have long looked for optimum depth resolution from RBS by using glancing beam incident or exit geometries to geometrically enhance the path lengths and hence the energy loss in thin surface layers. Williams & Möller (1978) gave a detailed analysis of the individual contributions to the energy resolution as a function of depth two decades ago. We show here how the more accurate calculations carried out by the DEPTH code of Szilágyi, Pászti & Amsel (1995), can be incorporated into high resolution RBS (HR-RBS) measurements on SiGe multilayers. DEPTH has been validated at the 10% level for many systems including pure Si (Szilágyi & Pászti, 1994), Co/Re multilayers (Barradas, Soares *et al*, 1994), and Si/Ge multilayers (Barradas, Jeynes, Mironov *et al*, 1998).

SiGe Multilayers: Integrated optoelectronics on silicon using a process compatible with current silicon technology would revolutionise the industry. There is consequently intense interest in possible materials and technologies for this. We have already mentioned β -FeSi₂: another possibility is the use of SiGe_x alloys, which can be grown coherently on a Si substrate for a variety of heterojunction devices. Because of the mismatch of the Si and Ge lattices these layers are heavily strained and must be very thin to be defect-free. Now the growers need to know not only the thickness and stoichiometry of their layers, but also the interface quality. It would be very desirable to do this by RBS if possible, since RBS is non-destructive for this type of sample, the measurements are rather rapid, and it is valuable to have an independent technique to compare with TEM and SIMS (both destructive techniques, with TEM being very time consuming as well).

Barradas, Knights *et al* (1999) have investigated a nominally (Si 30nm / Si_{0.78}Ge_{0.22} 5nm)*5 multilayer using HR-RBS. Our co-authors also used HR-SIMS and other techniques to characterise these samples. When the beam is incident normally on the sample the typical depth resolution for this system with RBS using, say, 1.5MeV He⁺, is about 40nm near the surface. But if a glancing angle of incidence is used the resolution (near the surface) can be improved to sub-10nm. The depth dependent energy resolution was calculated using the DEPTH code of Szilágyi *et al* (1995). We were able to obtain the probable Ge profile at sufficient precision to show that the probable mean layer thicknesses (characterising the interface roughness) change with growth temperature. Fig.9 shows the data for a multilayer grown at 550^oC, and the solutions compared for this sample and another grown at 810^oC.

Figure 7: Plots of the Fe/Si and Fe/Co ratios from an MCMC analysis of the mixed silicide spectrum in Fig.2 of Barradas, Jeynes & Webb, *Appl.Phys.Lett.* **71**, 1997, 291 (similar to Fig.2 in the present work). The solid contour lines marked "5", "6", "9" represent the 90, 95 and 99% confidence intervals respectively, calculated by MCMC. The axes are in thin film units (10^{15} atoms/cm²) and represent the total number of atoms of each species in the film

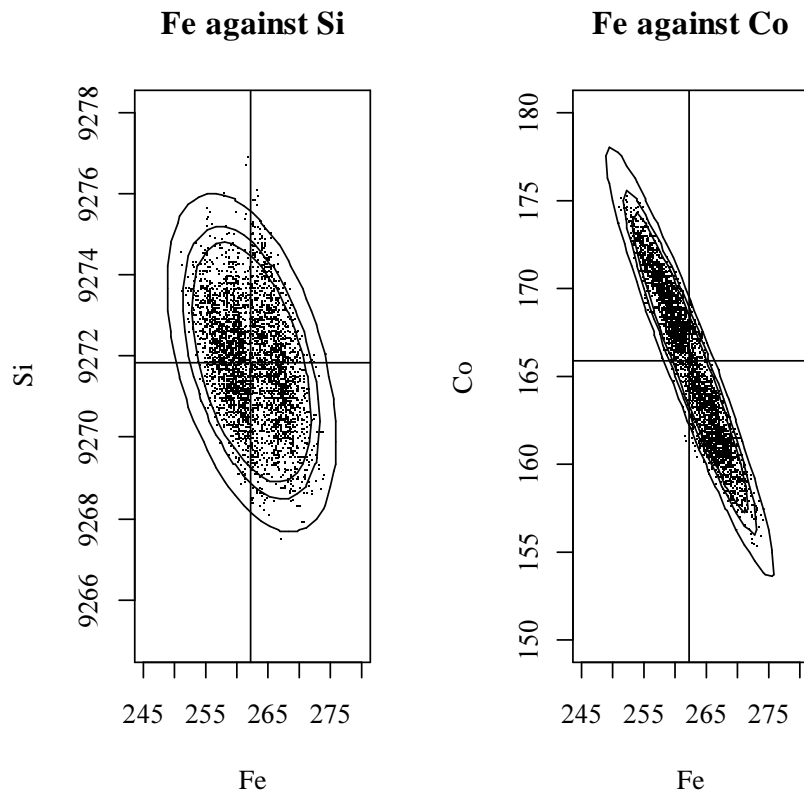
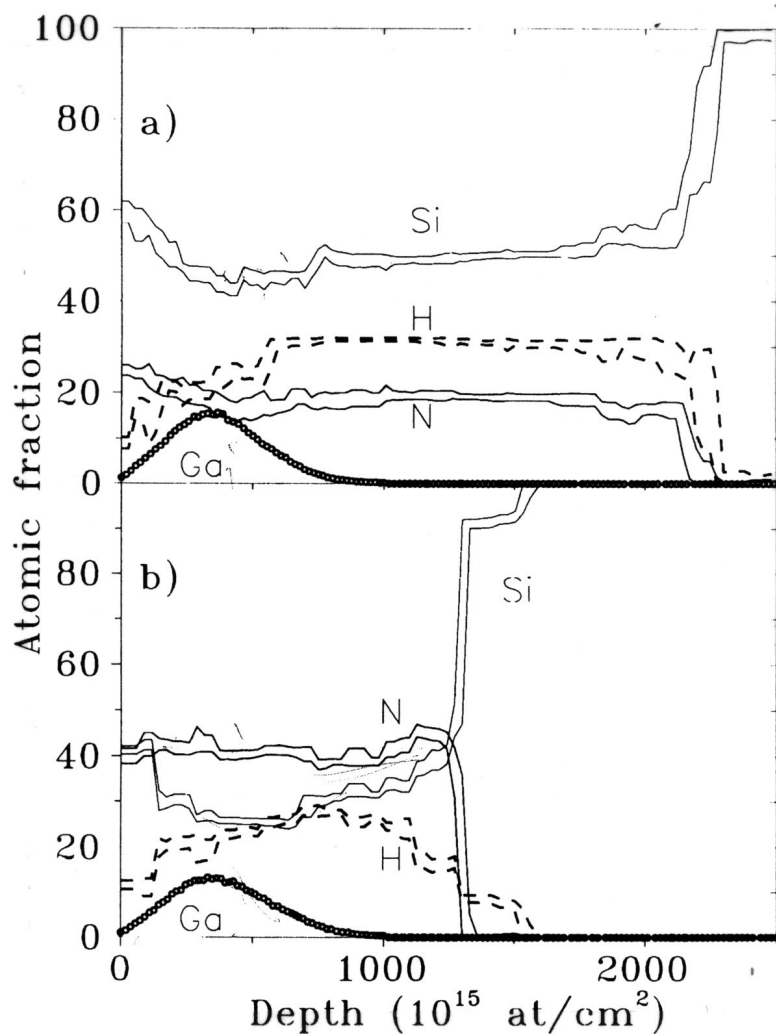


Figure 8: Confidence intervals of the Ga implanted samples of Fig.6 calculated by MCMC. **a)** Ga implanted into Si-rich SiN_x does *not* substitute preferentially for Si (shown in Fig.6); **b)** Ga implanted into Si-poor SiN_x (not shown in Fig.6) *does* substitute preferentially for Si (forming GaN, as shown by XPS); Fig.2 of Barradas, Almeida *et al*, Nucl. Instr. Methods **B148** (1999) 463-467.



The solution in Fig.9e showing the probable layer thicknesses indicates that there is a systematic increase in the layer thicknesses for the low temperature film. Fig.10 shows the error on the profile calculated with the MCMC method (similarly to the example of GaN:H shown in Fig.8 and described above): again, the indication given by SA is confirmed by MCMC.

High Depth Resolution by RBS? This very remarkable example deserves detailed discussion. The first general question is, how can useful information about the interfaces of films 5nm thick be obtained with a system whose declared depth resolution at the film surface is 7.5nm? The first answer to this is that while a depth profile will be broadened by the system resolution, and fine details will be smeared out, information about *moments* of distributions are available at *much* greater precision than the system resolution. For example, IBA analysts use this all the time to determine the electronics gain: we routinely achieve a precision in the determination of the position of surface signals a factor of 20 better than the nominal energy resolution of the system (cf. Seah *et al* 1988, Jeynes *et al*, 1998). The second answer is that in principle the system resolution function can be deconvoluted out of the data. This can be done indirectly as we do in this example, by including the depth dependent energy resolution in the forward model. As we have already pointed out, it can also be done directly using maximum entropy (Bayesian) techniques (Fischer *et al*; 1997, 1999) with astonishingly good results but at the cost of considerable computational difficulty.

Accuracy: The second general question is, how confident can we be of the accuracy of the result? We are, after all, putting considerable weight on the interpretation of very small features of the data. There are two aspects to accuracy: the relative accuracy (that is, the precision) of two profiles, and the absolute accuracy of a profile. The *relative* accuracy reflects the confidence with which we can discriminate differences between samples and which we have discussed in detail in the section on Bayesian techniques and which has been calculated for Fig.9 in Fig.10. To estimate the absolute accuracy implies a full error analysis as described below in the sections on accuracy and on the forward model limitations.

Use of the DEPTH code: The DEPTH code of Szilágyi *et al* is central to including accurate energy resolution values into the forward model. If this is not done correctly it is not possible to fit the data properly, and the objective function starts to become meaningless since it merely reflects forward model shortcomings. DEPTH calculates the energy resolution as a function of depth due to instrumental factors such as the beam energy width and the detection system resolution, the geometrical broadening in the detector due to finite detector solid angle, finite beam spot size and angular spread; and the energy straggling and multiple scattering which are the factors dependent on the sample. Although the simulation code RBX of Kótai (1994) effectively incorporates DEPTH internally, other simulation codes use Bohr straggling as an approximation to the energy straggling function, with a user-supplied factor to correct the values. This is quite unsatisfactory, especially as the functional form is not necessarily accurate. Multiple scattering is the excess energy straggling due to multiple low angle collisions. The DEPTH code does not calculate the low energy tails and other effects due to plural scattering, that is, multiple *large* angle collisions. Of course, plural scattering effects cannot be represented as a depth dependent energy resolution effect: plural scattering gives the specific spectral distortion of low energy tailing. This is outside the scope of this review, except to say that our MS correction will in many cases (including that of Fig.4) also adequately correct for plural scattering in an *ad hoc* way.

DEPTH directly calculates the energy resolution as a function of depth, assuming a particular

sample structure. Therefore in principle the calculation is implicit, relying on iteration to complete it. The sample depth profile must first be extracted from the spectrum without the depth resolution function, then the DEPTH calculation is done using this approximate profile, and then the SA is done again using the energy resolution function calculated by DEPTH. In fact, it was not necessary to iterate since there is very little difference between the energy resolution function calculated with and without the correct profile. However, including the depth dependent energy resolution function in the forward model considerably increases the forward model computation time, and therefore also the DataFurnace calculation time (which can be hours) since the forward model is at the core of SA.

Information from Multiple Spectra: In Fig.9, the multilayer cannot be resolved with the beam at normal incidence (Fig.9a). Even with a glancing incidence angle of 26° (Fig.9b) the layers are only partially resolved. However, as the glancing angle is decreased the Ge starts to overlap with the Si signal and the signal to noise ratio for the deepest layers decreases. Thus, for a glancing angle of 16° (Fig.9c) there is most information about the top three (or four) layers, whereas for 11° (Fig.9d) there is most information about the top two layers. DataFurnace handles all these spectra together self-consistently, with the highest resolution information being available about the top two layers. Notice that the overlap of the Si and Ge signals in Fig.9d causes a complex spectrum. Notice too that the spectrum is dramatically broadened for the deeper layers, and that the DEPTH calculation accounts for this correctly. This work is therefore a validation of DEPTH since unless the depth dependent energy resolution function is correctly calculated a good fit to the spectra at all angles of incidence will not be available simultaneously.

The result is shown in Fig.9e, which also shows a profile from a second sample grown at the higher temperature. These profiles are *consistent* with the data. As discussed above, the solution is given in terms of the minimum numbers of layers and compositions consistent with the data. What we fit is an estimate of mean layer thickness, equivalent to a second moment of the distribution. The energy resolution is convoluted into the spectrum calculated from the profile: the worse the energy resolution is, the less sensitive to small changes in the profile the data will be.

Error Estimate by MCMC: Thus, the suggestion in Fig.9e that the fourth and fifth layers merge into each other must be tempered with the knowledge that we do not have much information about these layers: many other profiles may also be consistent with the data. Again, we apply a Bayesian analysis of the expected error in these profiles and obtain Fig.10. Now the likelihood that the profiles from the two samples are really different can be evaluated more quantitatively. The samples grown at the lower temperature *do* have rather thicker layers at lower average Ge content, consistent with the interface broadening inferred from Raman spectroscopy. What is not included in this plot is estimates of the probable number of Ge atoms in each layer together with layer thicknesses and estimates of the error on these estimates. This information is also available to the user from the Markov chain calculation.

14- Non-resonant NRA

Workers at Surrey (Payne *et al*, 1989) were the first to use deuteration and the $D(^3\text{He,p})^4\text{He}$ reaction to follow the intermixing of polymers, although Lennard *et al* (1993) have thoroughly described the profiling of D using a ^3He beam in various Zr-based alloys. Barradas & Smith

Figure 9: *above:* Normal incidence and HR-RBS data of a nominally $(\text{Si } 30\text{nm} / \text{Si}_{0.78}\text{Ge}_{0.22} \text{ 5nm})_{\times 5}$ multilayer grown by MBE at 550°C . The solid lines are the fits and the dotted lines are the Si and Ge partial spectra. $1.5\text{MeV } ^4\text{He}$ and detector in Cornell geometry with scattering angle of 160° . *below:* Fitted Ge depth profiles for the data shown (550°C , dashed line) and for 810°C (solid line). The depth resolution function is calculated with the DEPTH code (Szilágyi, Pászti & Amsel, 1995). Figs.2&4 of Barradas, Parker *et al*, Phys.Rev. **B59** (1999) 5097-5105

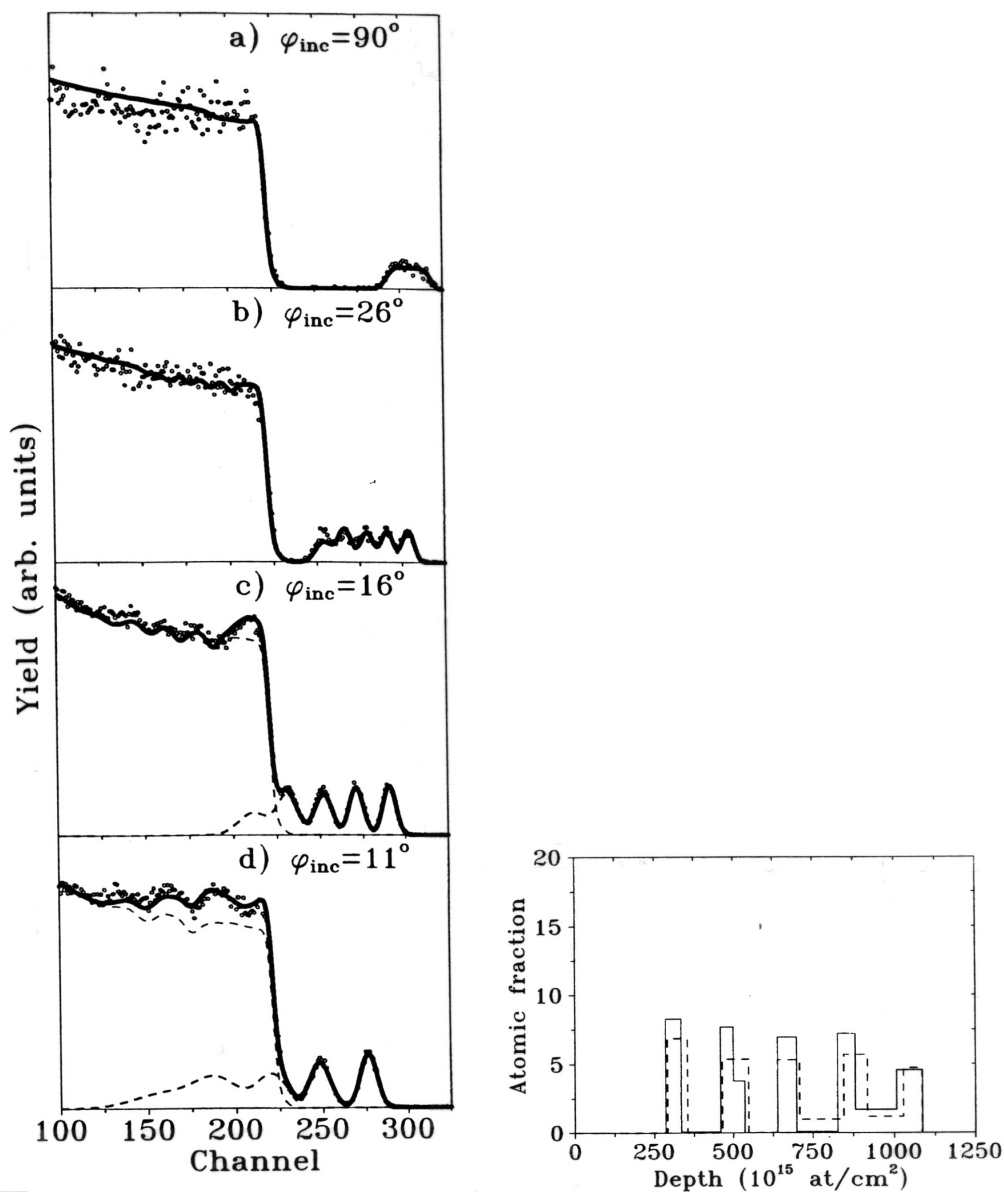
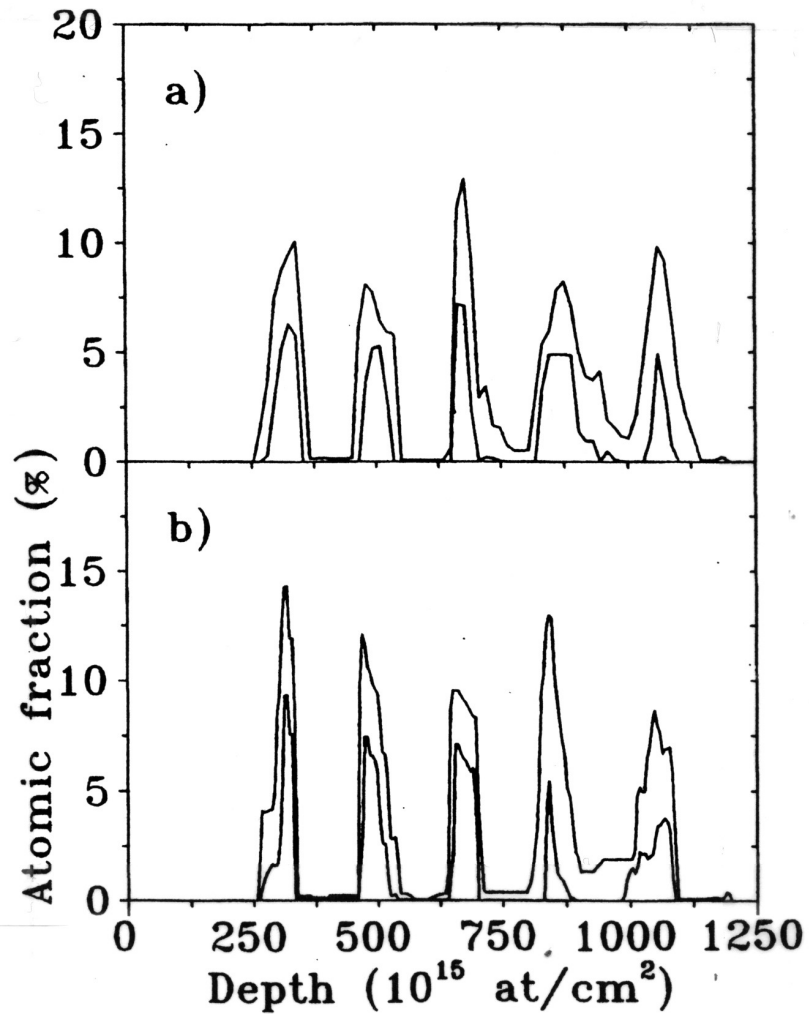


Figure 10: MCMC error calculation for the two samples of Fig.9e. Multilayers grown at **a)** 550°C and **b)** 810°C. Fig.6 of Barradas, Parker *et al*, Phys.Rev. **B59** (1999) 5097-5105



(1999) describe the analysis with DataFurnace of a multilayer of (hydrogenated) polystyrene (PS) and deuterated polystyrene (DPS) with a very high depth resolution of <6nm. DEPTH (Szilágyi *et al*, 1994, 1995) was essential for this work. The calculation of confidence intervals with MCMC confirms the multilayer structure.

Functionalised polystyrene blends have been analysed by Wendler *et al* (1999) using a very complete analysis first by simultaneous NRA/RBS with a ^3He beam and then by ERD/RBS. ^4He ERD of deuterated polymers using a detector with a range foil yields recoil spectra where the D and H recoil signals overlap. As mentioned above, the DataFurnace code handles this case too. All glancing incidence work, including ERD and high resolution analysis, depends on a very good knowledge of the geometry of the analysis. This geometry can be determined as one of the parameters of the data analysis if multiple spectra are collected at different beam incidence angles (since relative incidence angles are known more accurately than absolute ones). This approach is powerful in determining the *accuracy* of the analysis (that is, yielding a result which can be certified by reference to international standards) since the data themselves imply the instrumental parameters. However, a large number of spectra are collected: in this case we have analysed at least 13 per sample.

Barradas, Parascandola *et al* (1999) show an analysis of a nitrided steel by NRA/RBS with a 1.4MeV D beam and ERD with a 35MeV Cl beam. Two separate analyses were made by ERD, one using a standard ToF detector and the other an angle-resolving ionisation chamber. The NRA reaction was the $^{14}\text{N}(\text{d},\alpha_1)^{12}\text{C}$ with $Q=9.146\text{MeV}$. This looks deepest into the sample but with a poorer depth resolution than the ERD. Three different N profiles were thus obtained with different depths of analysis: these are handled together self-consistently by the DataFurnace which automatically weights the data from each spectrum according to its individual sensitivity.

15- Accurate IBA

The *precision* of an analysis, that is where *similar* samples are *compared*, has been considered above. However, the ultimate consideration of all analysis is the accuracy available. We use *accuracy* here in the critical sense, that is where a measurement can be traced back to international standards of mass, length and time with a specifiable uncertainty. Because the Rutherford cross-section is analytical the accuracy of RBS is potentially unlimited - except for the major problem in all IBA, the limited knowledge of the energy loss of ions in matter that we consider in detail in the next section. However, there are certain sorts of analysis where the energy loss enters only in second order: one of these cases has been treated in detail by Jeynes, Jafri *et al* (1997) with the conclusion that even in this ideal case there are several small effects that have to be considered (at the ¼% level) that will cumulatively make an *accuracy* better than 1% hard to achieve. (We quote all errors here at the 1σ confidence level.)

The only query about the potential accuracy of RBS to our knowledge is the interpretation of the low energy tails in backscattering spectra. Tails are certainly caused by multiple and plural scattering effects and have been calculated successfully with Monte Carlo techniques by Bauer *et al* (1992, 1993), and most recently by Eckstein & Mayer (1999) for low energy beams where the effects are large. They could also be caused both by slit scattering and any low energy component there may be in the beam. However, a careful experiment by Gurbich (1995) used time of flight techniques with a high energy pulsed beam (2MeV protons) and very thin foils (self-supporting gold at about 10keV thick for this beam), with the result that he found large

unexplained tails, at about 10% of the size of the expected backscattering from the thin foil.

We point out, parenthetically, that we believe that it is harder than generally supposed to establish the energy calibration with an accuracy better than 1%. Although the machine energy can be established readily at about 0.1%, the electronics calibration depends on an accurate knowledge of the pulse height defect of the detector. This has been comprehensively described recently by Lennard, Tong *et al* (1990), and we have presented a full analysis in a particular case where the best demonstrable accuracy was only 0.5% (Jeynes, Barradas, Blewett & Webb, 1998). Lennard *et al* (1999) do not make a comparable accuracy estimate explicitly, but their work is consistent with an accuracy of about 0.5%. We are not aware of any other work that establishes the energy calibration accuracy.

Apart from issues of energy calibration, accuracy in RBS turns on knowledge of the product of the detector solid angle and the collected charge, the so-called charge.solid-angle product, since very careful work from two decades ago established the validity of the analytical RBS cross-section when the electron screening effect was taken into account. The accuracy of the corrected RBS cross-section is usually better than the ½% cited by Wätjen *et al* (1992) for the worst case of Bi, which is of course very heavy. Solid angle is troublesome to measure accurately at the 1% level, as is routine charge collection in RBS systems, and analysts have used standard (certified) samples for a decade to avoid routine use of absolute values of charge and solid angle.

The existing standard samples are Bi implants into Si, the Bi contents of which are now certified at 1.3% (Wätjen *et al*, 1994; Wätjen, 2000). A new set of Sb implanted samples are now available from IRMM, Geel and BAM, Berlin, and are certified at 0.6% (Ecker *et al* 2002).

Implanted silicon standards: Very recently there has been useful work on new standard samples, where the measurand is the surface yield of an implanted (amorphised) silicon sample (Lennard *et al*, 1999; Bianconi *et al*, 2000) This is equivalent to an absolute measurement of the energy loss of Si (see Konac *et al*, 1998, and the discussion in Barradas, Jeynes, Webb & Wendler, 2002). In Bianconi *et al's* work two labs made absolute measurements of the charge.solid-angle product, at nominally 1% accuracy, and got agreement within the stated error. The traceability of Lennard *et al's* work is not so easy to establish, but they obtain the same values. Niemann *et al* (1996) have also made measurements of energy loss in Si at an accuracy approaching 1%. The point here is that Bi or Sb implant samples are specific artefacts, but every lab can make their own amorphised Si samples on demand. Secondary standards must be used systematically with the Bi certified standards, with the associated error and complexity; not so for the amorphised Si. The difficulty with certifying the Bi implants has been in establishing the real variation across the implant batch, but the uniformity and purity of modern production silicon ingots has been established at extraordinary sensitivity and accuracy: modern standard RBS samples can now take advantage of this.

It should not surprise the reader, bearing in mind the preceding discussion, that much current routine RBS has difficulty *establishing* an accuracy better than 10%. Critical work is usually done *relative* to internal standards in the sample set: the accuracy of such work is usually very difficult to trace.

Boudreault *et al* (2002) have now demonstrated an RBS analysis at an accuracy *certifiable* near the 1% level, traceable through the new IRMM/BAM standard samples, and which could be implemented as a routine tool. Heavy ion implants into silicon can be chosen to leave the surface

implanted layer fully amorphised. Standard implants like these are important in implantation labs for validating the implanter performance. Therefore a routine certifiable analysis is of considerable value.

Two detectors at different scattering angles are used. The DataFurnace is used to calculate the depth profile as described above: this calculation is done self-consistently using correct stopping powers (we remind the reader that most widely used codes do not do a proper self-consistent calculation, giving an error that increases with As concentration). The pileup correction of Jeynes, Jafri *et al* (1997) is used. The integration of the As profile gives the As atom density directly. Clearly, such an analysis is traceable not only to the *value* of the stopping powers at the energy of analysis but also to the *shape* of the energy loss as a function of energy (although for low energy implants a single correction value is adequately accurate). The new accurate values of the energy loss function in silicon are easily included explicitly in the DataFurnace energy loss database, making a fully traceable *routine* analysis straightforward.

The interesting thing about this approach is that the spectra from both detectors are handled together self-consistently: this is equivalent to two essentially independent measurements of the same quantity (given the accelerator parameters of course). Not only this but also the data reduction is automatic. Thus we demonstrate a rapid routine automatic analysis of certifiable accuracy where a single measurement contains its own validation with information from two independent data channels. In the case shown the two detectors give respectively $861.10^{12}\text{As/cm}^2$ and $855.10^{12}\text{As/cm}^2$ with a difference of about 0.8% consistent with the counting statistics. The values are about 1% lower if infinite As dilution is assumed, emphasising the importance of a correct calculation. The accuracy of the electronic energy calibration (independently determined for each detector) is important, since it is comparable to the counting statistics only if carefully done. The charge.solid-angle product is determined absolutely (again, independently for each detector) from the standard value used for the energy loss.

Elastic (non-Rutherford) scattering: We have recently demonstrated a very good precision of 2% and quite a good accuracy of 10% in a determination of the C content of Ni-Ta-C magnetron-sputtered films on a silicon substrate using a mixed EBS/RBS analysis and a 1.75MeV H beam (Jeynes, Barradas & Wilde, 2000). These films were very uniform and reproducible, and it was possible, assuming their uniformity, to use a transparent (and hence traceable) manual method for data reduction to obtain the stoichiometry. The difficulty with EBS is the very strongly non-Rutherford cross-section for both the C and the Si signals. Not only can the cross-section enhancement be very large (peaking at a factor of about 60 for C for a proton beam of 1.737MeV) but the variation with energy can be equally large. The paper includes a discussion of the cross-sections, which are outside our present scope. The successful use of EBS for accurate analysis clearly depends on accurate cross-sections. However, it also depends on codes that can effectively implement these cross-sections. H EBS is hard to use with traditional data reduction methods since there is usually considerable elemental overlap even with simple samples. DataFurnace is therefore particularly valuable for extracting depth profiles from H spectra. In this case we were able to demonstrate the validity of the assumption of uniformity of the films that was made for the manual analysis. The DataFurnace and the manual analysis agreed at the analysis precision. This is not necessary: the data reduction algorithms for the two methods are independent (although of course the same energy loss values and instrumental parameters are used for both analyses). This work is an important validation of the DataFurnace

code.

It is worth remarking that these data have also been successfully analysed by an artificial neural network (ANN) code (Vieira & Barradas, 2001), relying on the accuracy of the DataFurnace analysis to validate the ANN methods.

Microbeam RBS: An interesting example of an accurate analysis is the recent microbeam analysis of copper containing deposits printed with an inkjet (Jeynes *et al*, 2002; Rozenberg *et al*, 2002): the inkspots were about 300 microns across and very non-uniform needing a beam spot size of 10 microns. Again the RBS spectra were ambiguous, with the added problem that the true collected charge had to be determined from the spectra themselves (a standard problem with the microbeam). We were able to demonstrate from the objective goodness of fit (the χ^2 function) for a range of possible inkspot compositions that the inkspots were at least 90% copper by weight.

Conclusion: Analytical accuracy depends in all cases on being able to objectively estimate the confidence interval for the results. DataFurnace is the only code that can do this reliably for the general IBA data we have been describing, using the MCMC methods we have described above (Fischer *et al*'s MaxEnt code appears to be too cumbersome for general purpose use). The simple statistics we currently use on the MCMC data are very well suited for this purpose. However, more mathematical work is required to fully validate the cooling schedule and other details of both the MCMC and the SA algorithms.

16- Forward Model Extension: Roughness

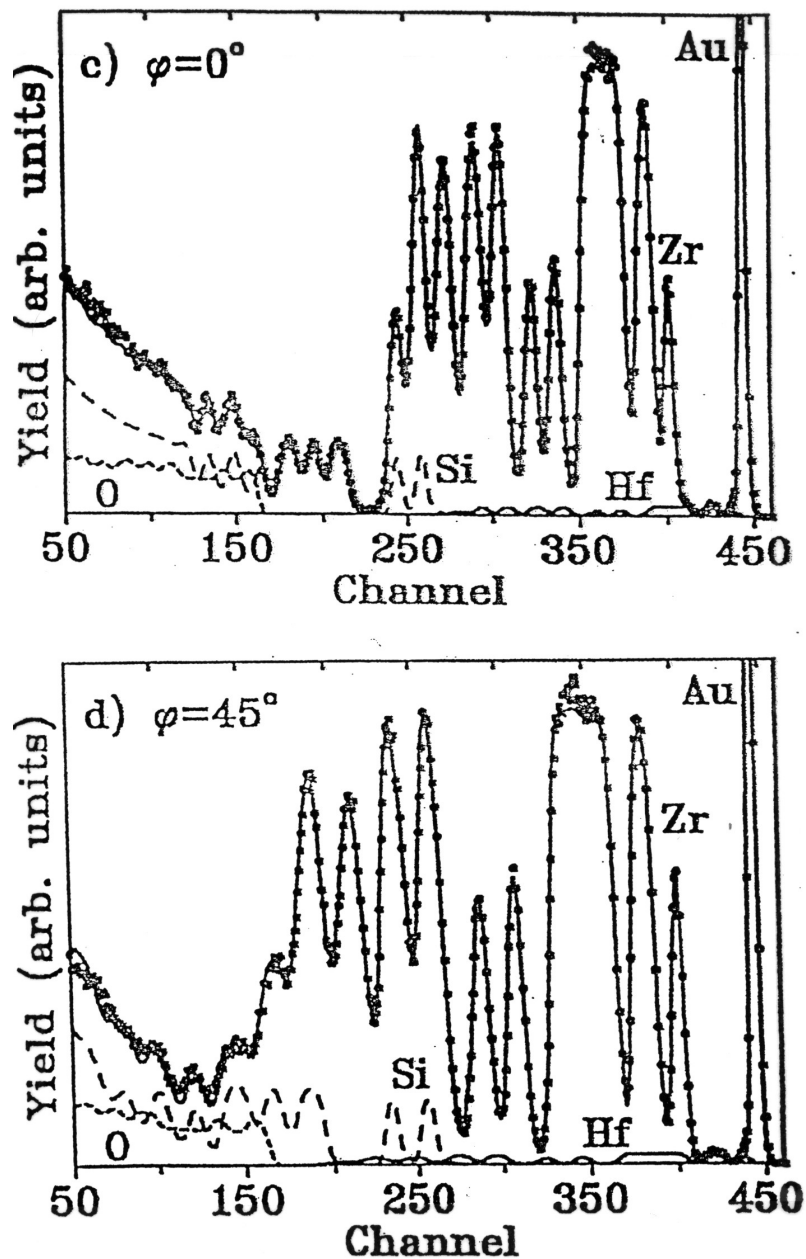
Another effect is *surface topography*. This introduces marked spectral distortions which cannot be evaluated without a model, introducing many more parameters in the description of the sample. These effects have been long known: a notable example is Edge's (1983) elegant use of them to characterise optical fibres and optical gratings.

Roughness problems are attracting increasing attention now that computers are so much faster, for example: Marin *et al* (1996) have extracted information about the distribution of the droplet sizes of lead on glass and copper in kapton and Niwa *et al* (1998) have done similarly for an island growth problem; Simon *et al* (1998) have analysed patterned and porous samples with the microbeam; and Slotte *et al* (2000) have shown how spectra from rough samples can be solved using IBA, AFM and SEM methods in a complementary way.

Systematic approaches have been made to the accurate calculation of spectra from general rough surfaces for RBS by Shorin & Sosnin (1992) using a Monte Carlo code and for ERD by Yesil *et al* (1998) with the SURF code.

Clearly these sorts of codes are too slow to incorporate into DataFurnace and Barradas (2001) has implemented a simple and generally useful parameterisation scheme for rough surfaces which is valid for moderate roughness, that is, provided the beam does not enter and leave the sample more than once. This approach is appropriate for thin films and multilayers with roughness values up to a few tens or hundreds of nm. By calculating the broadening due to roughness, and assigning it as an extra contribution to the energy straggling, an apparent energy resolution is obtained. This is then convoluted with the theoretical spectrum in the normal way. The effect of roughness can thus be included in NDF with little effort, paying only a small price

Figure 11: 2MeV 4He⁺ RBS data (dots) and DataFurnace fit (line) of the structure shown in Table 2. This is a 21 layer antireflection coating of silica and zirconia on glass. The DataFurnace fit assumes molecules (no free oxygen), where the zirconia has a Hf contamination. The energy resolution as a function of depth is calculated with the DEPTH code of Szilágyi, Pászti & Amsel, 1995. Two angles of beam incidence are used sequentially with the data fitted simultaneously. Partial spectra for Hf, Si and O are also shown. From Fig.2 of Jeynes et al, Surf.Interface Anal. 30, 2000, 237



in terms of calculation time.

The broadening depends on the exact type of roughness. Three different models were implemented into DataFurnace: inhomogeneous layer thickness, corrugated sample and rough substrate surface (refer to Figure 4 of Barradas, Soares *et al*, 1994, for a visualisation of the models: this example has been reanalysed with the modified NDF code in Barradas, 2002). Interfacial mixing in multilayers can also be analysed with the method developed - see Barradas, Sequeira *et al* (2002) for an example in the SiGe system and Tavares, Rebouta *et al* (2002) for one in the TiAlN/Mo system. DataFurnace can perform automatic fits to several spectra collected from the same sample, ensuring all the information in the data is used self-consistently to obtain the final depth profile and roughness parameters. The code is also valid for ERD.

17- Forward Model Limitations: Stopping Powers (Optical Multilayers)

The analysis of samples like optical filters make a dramatic demonstration of the power of these new techniques. Jeynes, Barradas, Rafla-Yuan *et al* (2000) have described the analysis of a 21 layer anti-reflection coating consisting of a silica/zirconia stack on a glass substrate using 2.2MeV ⁴He RBS (Fig.11). Using the proper depth dependent energy resolution function we could demonstrate a perfect self-consistent fit to double detector data (actually this data was single detector, but with two incident angles of the beam). An MCMC analysis was carried out, and deep in the stack, at a depth of a micron, we find that, for example, the 17th layer (zirconia) is 30.0 ± 2.6 nm thick, where the error has a confidence of 95%.

We should note that the MCMC information is now being treated in a different way from the simple display as in Figs.8 & 10 for example. The fit was carried out allowing the zirconia and silica to mix (no solution is available if mixing is not allowed). The errors calculated by MCMC are available as a function of depth. Equivalent pure layer thicknesses are calculated, with their errors, by splitting the "mixed" regions equally between their pure neighbours.

This analysis was carried out using the information that only zirconia and silica are present in the stack: we used three molecules, ZrO₂ (with a Hf contamination), SiO₂ and the five element float glass substrate including 0.2 at% Sn which significantly complicates the spectra. Thus although 7 different elements are significant in the sample only three molecular fitting parameters are used, and the light element O is always correlated with heavier elements with larger signals. We shall see that in fact this correlation of the low and high energy parts of the spectrum is also essential to obtain a correct solution for another reason. Clearly with such a complicated sample it is very desirable to restrict the state space with as much prior information as is available.

It is astonishing that such a precision (better than 3nm) is available so deep in such a complicated sample. For comparison, the detector energy resolution at around 12keV is equivalent to a depth in silicon of about 30nm. Energy straggling should rapidly degrade this with depth. Of course, the precision of the layer thickness calculation is not the same as an objective evaluation of the true depth resolution. We have already noted that many quantities can be determined at a precision much better than the nominal depth resolution. In this case we have imposed the assumption of sharp interfaces onto the sample, and we are effectively counting atoms per layer, something RBS is extremely good at.

The question then arises: what is the *accuracy* of the determination of the layer thicknesses? For thin films the answer is simple: counting atoms simply depends on the accuracy of the

system calibration. However, for thick films we have to consider the effects of the enhanced backgrounds and the spectral distortions caused by multiple and plural scattering effects. Some of these effects can be largely eliminated with standard analytical methods as described above, but complex spectra like these will be very sensitive to them. This is as yet an open problem since what is needed is well founded analytical approximations for these effects that can be incorporated into SA.

If on the other hand we ask what is the confidence we have in the *interface* information (recall that the fit insisted on mixed interface regions) the answer is very different. We tried initially to fit these spectra with an old code that did not permit molecules. We found that solutions were very easy to find, but that they always involved *no* correlation between the oxygen and the metals. The elemental solutions did not give the right stoichiometries. It turns out that where there are strong interface signals SA is *extremely* sensitive to the system calibration. Moreover, the position of the interface signals is determined by energy loss. Therefore any error in the energy loss function of one element that is not exactly matched by corresponding errors in all the other relevant elements will make the code want to put the interface signals for the different elements in different places. Where the elemental signals are not correlated by the use of molecular parameters the real correlation between elements will be obscured by the errors in the energy loss database. Similarly, where molecular parameters are used, interface information will also be obscured. Therefore we suspect that the insistence of the DataFurnace that the interfaces are *mixed* is probably an artefact due to errors in the stopping power database.

18- Other Examples

DataFurnace has been used for a variety of materials analyses. It is worth giving a list here.

The Lisbon group have used high resolution RBS to monitor the fabrication of MnIr spin valves with nano-oxide layers formed from plasma oxidation of CoFe layers (Veloso *et al*, 2000). This process is to enhance the magnetoresistance for magnetic memory application. Zhang *et al* (2001) have investigated processing problems with magnetic tunnel junctions (used for magnetic random access memory applications) fabricated with sophisticated metallic (and semi-metallic) multilayers and analysed with high resolution RBS.

The group at Surrey has also: measured lateral stress in implanted gold films using a three crystal quartz resonator method and a detailed self-consistent RBS analysis (Way *et al*, 1999); investigated surfactant behaviour in the formation of latex films (Tzitzinou *et al*, 1999); characterised sol-gel deposited Ta₂O₅ and TiO₂ dielectric films on silicon (Cappellani *et al*, 1999); used complementary RBS and XPS to investigate tribological coatings (TiN, TiAlN and MoS₂:Ti) on steel (Baker *et al*, 2000); investigated low temperature growth of GaN (Young *et al*, 2000); and measured H and N content of a-C by Hi-ERD (at Rossendorf citing Barradas, Khan *et al*, 2000; Carey *et al*, 2000, 2001)

The Göttingen group has followed ion beam mixing of Si/C multilayers (Harbsmeier *et al*, 2000) and Ta/Si bilayers (Bibic *et al*, 2000) with RBS and other methods. The Darmstadt group has investigated heavy ion induced metal-ceramic interface diffusion with RBS (Nagel *et al*, 1999, 1999).

The Cambridge group has characterised silicon anodically oxidised using a wave resonance plasma (WARP) source by RBS (Uchikoga *et al* 1999), and also characterised WARP deposited a-C:N:H films by He ERD/RBS (Rodil *et al*, 2000). Other British RBS applications include the characterisation of gate oxides on SiGe MOSFETs (Riley *et al*, 1999: Liverpool / London / Southampton) and the profiling of silver nanoparticles formed in glass by high dose implantation (Stepanov *et al*, 1999: Sussex).

19- Future Developments: Turnkey IBA

Historically the use of IBA has been largely restricted to university research groups. There has been an explosion in the development of a large variety of beautiful techniques and there is no doubt of its utility in research. However, the impact on industry of IBA methods has been marginal, and we believe that this is largely due to the time and skill required to properly interpret even RBS data, the simplest of the IBA techniques. The new data reduction methods that we have described here are powerful enough to revolutionise IBA. In the future, turnkey benchtop accelerators will be operated by technical or graduate level staff (rather than research staff) and profiles will be generated automatically and on-line from the spectra. Staff training should take no longer than two or three days, and there will be well defined quality assurance procedures both for calibrating the instrument and presenting and validating data. Such instruments will still be limited by the skill of the operators, and research staff would be able to push the instruments much further. However, routine analysis will be available for a wide range of sample types at an accuracy certifiable at or near the 1% level, and at a fraction of the current cost. Immediately a wide range of analyses relevant to process development, production control and quality control become feasible and such simplified instruments will find widespread use.

EBS: We anticipate that the progress made recently in understanding the functional form of the EBS cross-sections (Gurbich, 1997, 1998, 1999) should allow a comprehensive database for these cross-sections to be loaded, and for the distinction between RBS and EBS to be transparent to the user. At present the use of EBS is badly hampered because the analyst must make sure that the scattering angles used conform to the angle for which the cross-sections were measured, but Gurbich's formalism will allow the interpolations from the database to any angle. Moreover, the Handbook (Tesmer & Nastasi, 1995) can be misleading and is not suitable for accurate work: a more reliable cross-section database is very desirable.

PIXE, VASE, NDP: So far we have not attempted to implement SA for *PIXE* data. *PIXE* and RBS are complementary: RBS frequently does not have unequivocal elemental identification and *PIXE* is rather insensitive to inhomogeneity in depth. The two together should be very powerful indeed. In principle the *PIXE* forward model should not be too hard to implement, we have not done this up to now since it is completely different physics from particle scattering. We should mention that just as *PIXE* could be implemented with a new forward model, so could other techniques. We have already explored the use of SA annealing with variable angle spectroscopic ellipsometry (*VASE*) (Barradas, Keddie & Sackin, 1999): this is a widespread and powerful technique to which IBA is complementary. We believe that a DataFurnace extension that allowed simultaneous self-consistent fitting of IBA and ellipsometric data would be

tremendously powerful. An extension to neutron depth profiling (*NDP*) has recently been implemented.

High depth resolution is of great current interest, with many important technologies dependent on the manipulation of very thin films. We have demonstrated that when combined with an accurate function of energy resolution with depth a DataFurnace analysis can yield an astonishing depth resolution for the most complex sample. We believe that SA could be used as a preprocessor for a maximum entropy code, since the computation time for such a code is dramatically reduced if the position of the solution in state space is approximately known. The drawback of this approach is that the detector transfer function must be accurately known, but the benefit would be a greatly enhanced depth resolution for a reasonable computation time. A sub-atomic depth resolution should be available if high resolution detectors (eg: Lanford *et al*, 1998) are used.

Neural Networks: A very interesting recent development, completely unrelated to simulated annealing, is in the demonstration that artificial neural networks (ANNs) can be effective and surprisingly accurate in interpreting RBS spectra (Vieira & Barradas, 2000, 2001; Barradas & Vieira, 2000; Barradas, Vieira & Alves, 2001). It has become clear that ANNs can only be used to interpolate, not extrapolate, the training set (Vieira, Barradas & Jeynes, 2001). The interesting thing about ANNs is that in operation they are entirely model-free - the ANN is a "black box" with a spectrum as input and the required parameters as output and there is *no* physics calculation in the box. The physics is all *implicit* in the set of spectra and their solutions used to train the ANN. Note that the calculation of the ANN is effectively *instantaneous*: there is no computation time to extract the programmed parameters from the spectrum. The prospect has been raised of "RBS without humans" (Barradas, Patricio & Vieira, 2002), but more realistically we can consider using ANNs in special situations where large numbers of similar spectra are to be analysed.

20- Future Developments: The Algorithm and the Forward Model

MCMC: Because of the pressure to have on-line analysis with multiple techniques, and because of the highly computationally intensive nature of both SA and the forward models (especially when the full depth dependent energy resolution function is incorporated), algorithmic issues will remain important. We expect significant increases in speed with a more efficient generation function, and although we currently use an adaptive cooling schedule we do not believe it is anywhere near optimal. Also the currently used local minimisation is slow. MCMC methods could be used for characterising the state space of spectra more systematically: looking for the set of near-optimal solutions, which may be effectively discontinuous as in our silicides example. This may enable priors to be specified more robustly. Of course, the MCMC calculation makes vast amounts of information available, from which we only extract a variance at present. This data could be treated in a more sophisticated way.

These ideas are explored by Marriott *et al* (2002), who have found a far more efficient algorithm than the one we currently use. They look at a different MCMC algorithm which is based on ideas from the Gibbs sampling formulation of MCMC rather than the Metropolis-Hastings method (simulated annealing) described here. This new method more fully exploits the information available in the forward model calculation (the elemental sub-spectra) to efficiently generate possible new states. The better the generation function the more efficient the MCMC.

Parallel Processing: MCMC (and therefore also SA) is easy to implement on parallel processor machines, and we expect that any serious increase in the industrial use of IBA techniques will also lead to very high specification hardware being used. After all, a £2K PC is only 0.2% of the cost of a £1M accelerator system.

Unresolved algorithmic issues include some *ad hoc* parameters such as the 1.5 exponent used for normalising the chisquared (Barradas, Jeynes, Webb, Kreissig, & Grötzschel, 1999), this means that we cannot yet demonstrate that we weight multiple spectra correctly. More important is the outstanding problem of continuity which represents important prior information about the sample that is rather hard to specify objectively. Has the sample got implant or diffusion profiles? How many layers does it have (we already estimate this from the derivative of the spectrum, but we are not convinced that an unequivocal algorithm exists)? What is the difference between a diffused interface and a diffusion profile? Progress in systematising these questions will greatly help the implementation of turnkey IBA.

Unresolved forward model problems: There are two major areas where the IBA forward model is unsatisfactory and progress in these will improve its accuracy. *Multiple & plural scattering* are well simulated with Monte Carlo methods. These effects become important for thick samples and for glancing angle IBA. The contribution to straggling of multiple straggling effects is estimated well by Szilágyi's DEPTH code, but its low energy background and the spectral distortion of plural scattering cannot yet be estimated simply. Some systematic analytical approximation will be very valuable. The *energy loss database* represents a huge amount of experimental and theoretical work, but its accuracy is still rather poor in general. We believe that with accurate data analysis for IBA now being available it may be possible to find much more rapid ways to obtain high quality energy loss data. In any case, accurate knowledge of energy loss is essential for accurate IBA.

21- Summary

Since the analysis of RBS spectra using simulated annealing methods was first published in April 1997 we have generalised the method to all the depth profiling (particle scattering) IBA techniques, and also supplied a highly usable interface for the analyst. We have called this the IBA DataFurnace. We have here reviewed the literature both on these developments and their context.

There are a very wide range of powerful IBA techniques in use in the scientific community, including (to mention just a few) ion channelling for the analysis of crystalline defects, ion beam induced current for *in situ* analysis of working integrated circuits, and microbeam analysis for lateral resolution. Extremely high lateral resolution is available from transmission ion channelling. "Simple" depth profiling may be the least interesting of these techniques, but it is very widely applicable by thin film technologists and materials scientists, and we have produced a code which takes the drudgery out of it.

The IBA DataFurnace amounts to a new and very powerful tool for depth profiling thin film samples.

Acknowledgements

This work was supported by the Surrey IBC under EPSRC contracts GRJ 97540, GRK56247 and GRL 78512. MJ was supported by EPSRC and by the National University of Singapore (grantholders PKM & F.Watts). We are grateful to Prof. B.J.Sealy for his encouragement and to Alex Gurbich for a careful and critical reading of a draft of the manuscript. We would also like to thank Chris Burt for skilfully operating the accelerator.

Figures

1. RBS of Fe implant in Si.	12
2. RBS of mixed Fe & Co implants in Si (Barradas, Jeynes & Webb, 1997)	14
3. RBS of ion beam mixed iron silicides (Barradas, Milosavljevic <i>et al</i> , 1998)	16
4. RBS of O implanted SiC (Barradas, Jeynes & Jackson, 1998)	23
5. Ambiguity in RBS oxidised NiCrAl alloy (see Butler, 1990)	27
6. RBS/ERD of Ga implanted SiN _x :H (Barradas, Almeida <i>et al</i> 1999)	29
7. MCMC correlation analysis of mixed silicide RBS	33
8. Depth profiles with MCMC of Fig.6 (Barradas, Almeida <i>et al</i> 1999)	34
9. HR-RBS of Si:Ge multilayer (Barradas, Parker <i>et al</i> , 1999)	37
10. Depth profiles with MCMC of Fig.9 (Barradas, Parker <i>et al</i> , 1999)	38
11. RBS of anti-reflection coating (Jeynes <i>et al</i> 2000)	43

References

12. E.Aarts, J.Korst, Simulated Annealing and Boltzmann Machines: *A Stochastic Approach to Combinatorial Optimization and Neural Computing* (John Wiley & Sons, Chichester, 1989)
13. P.F.A.Alkemade, F.H.P.M.Habraken, W.F.van der Weg, *On the ambiguity in the analysis of Rutherford backscattering spectra*, Nucl. Instr. and Methods **B45** (1990) 139-142
14. S.A.Almeida, S.R.P.Silva, B.J.Sealy, J.F.Watts, *Bond formation in ion beam synthesised amorphous gallium nitride*. Thin Solid Films **343-4** (1999) 632-636
15. G.Amsel, *CUTBA - Cleaning up the Tower of Babel of Acronyms in IBA*, Nucl. Instr. and Methods **B118** (1996) 52-56
16. G.Amsel, M.Menu, J.Moulin, J.Salomon, *The 2MV tandem pelletron accelerator of the Louvre Museum*, Nucl. Instr. and Methods **B45** (1990) 296-301
17. M.A.Baker, S.J.Greaves, E.Wendler, V.Fox, *A comparison of in situ polishing and ion beam sputtering as surface preparation methods for XPS analysis of PVD coatings*, Thin Solid Films **277-278** (2000) 473-477
18. N.P.Barradas, *Rutherford backscattering analysis of thin films and superlattices with roughness*, J.Phys.D **34** (14) (21July 2001) 2109-2116
19. N.P.Barradas, *Fitting of RBS data including roughness: application to Co/Re multilayers*, IBA-15, Nucl.Instr. and Methods **B190** (2002) 247-251
20. N.P.Barradas, S.A.Almeida, C.Jeynes, A.P.Knights, S.R.P.Silva, B.J.Sealy, *RBS and ERDA simulated annealing study of ion beam synthesised gallium nitride*, Nucl. Instr. and Methods **B148** (1999) 463-467
21. N.P.Barradas, C.Jeynes, M.A.Harry, *RBS/simulated annealing analysis of iron-cobalt silicides*, Nucl. Instr. and Methods **B136-138** (1998) 1163-1167

22. N.P.Barradas, C.Jeynes, K.P.Homewood, B.J.Sealy, M.Milosavljević, *RBS/simulated annealing analysis of silicide formation in Fe/Si systems*, Nucl. Instr. and Methods **B139** (1998) 235-238
23. N.P.Barradas, C.Jeynes, S.M.Jackson, *RBS/simulated annealing analysis of buried SiCO_x layers formed by ion implantation of O into cubic silicon carbide*, Nucl. Instr. and Methods **B136-138** (1998) 1168-1171
24. N.P.Barradas, C.Jeynes, M.Jenkin, P.K.Marriott, *Bayesian Error Analysis of Rutherford Backscattering Spectra*, Thin Solid Films **343-344** (1999) 31-34
25. N.P.Barradas, C.Jeynes, Y.Kusano, J.E.Evetts, I.M.Hutchings, *RBS/simulated annealing and FTIR characterisation of BCN films deposited by dual magnetron sputtering*, **CP475**, Applications of Accelerators in Research and Industry (eds. J.L.Duggan, I.L.Morgan) AIP 1999, pp504-507
26. N.P.Barradas, C.Jeynes, O.A.Mironov, P.J.Phillipps, E.H.C.Parker, *High depth resolution Rutherford backscattering analysis of Si-Si_{0.78}Ge_{0.22}/(001)Si superlattices*, Nucl. Instr. and Methods **B139** (1998) 239
27. N.P.Barradas, C.Jeynes, R.P.Webb, *Simulated annealing analysis of Rutherford backscattering data*, Appl.Phys.Lett. **71** (1997) 291-3
28. N.P.Barradas, C.Jeynes, R.P.Webb, U.Kreissig, R.Grötzschel, *Unambiguous automatic evaluation of multiple ion beam analysis data with simulated annealing*, Nucl. Instr. and Methods **B149** (1999) 233-237
29. N.P.Barradas, J.L.Keddie, R.Sackin, *Bayesian inference analysis of ellipsometry data*, Phys.Rev.E **59** (1999) 6138-6151
30. N.P.Barradas, A.P.Knights, C.Jeynes, O.A.Mironov, T.J.Grasby, E.H.C.Parker, *High-depth-resolution RBS data and error analysis of SiGe systems using the simulated annealing and Markov Chain Monte Carlo algorithms*, Phys.Rev.B **59(7)** (1999) 5097-5105
31. N.P.Barradas, P.K.Marriott, C.Jeynes, R.P.Webb, *The RBS DataFurnace: Simulated annealing*, Nucl. Instr. and Methods **B136-138** (1998) 1157-1162
32. N.P.Barradas, S.Parascandola, B.J.Sealy, R.Grötzschel, U.Kreissig, *Simultaneous and consistent analysis of NRA, RBS and ERDA data with the IBA DataFurnace*, Nucl. Instr. and Methods **B161-163** (2000) 308-313
33. N.P.Barradas, A.D.Sequeira, N.Franco, M.Myronov, O.A.Mironov, P.J.Philips, E.H.C.Parker, *RBS analysis of MBE grown SiGe/(001)Si heterostructures with thin high Ge content SiGe channels for HMOS transistors*, Mod.Phys.Lett. **B 15** (2001) 1297-1304
34. N.P.Barradas, R.Smith, *Simulated annealing analysis of nuclear reaction analysis measurements of polystyrene systems*, J.Phys.D **32** (1999) 2964-2971
35. N.P.Barradas, J.C.Souares, M.F.da Silva, F.Pászti & E.Szilágyi, *Study of multilayer substrate roughness using RBS with improved depth resolution*, Nucl. Instr. and Methods **B94** (1994) 266-270
36. N.P.Barradas, R.P.Webb, C.Jeynes, *WiNDF: a windows interface to the DataFurnace code for analysing IBA data*, Presented at IBA14 (Dresden, July 1999). Text available on: www.ee.surrey.ac.uk/SCRIBA/ndf
37. N.P. Barradas, C. Jeynes, R.P. Webb, E. Wendler, *Accurate determination of the stopping power of ⁴He in Si using Bayesian inference*, Nucl. Instr. and Methods **B194** (2002) 15-25
38. N. P. Barradas, A. Vieira, *Artificial neural network algorithm for analysis of Rutherford backscattering data*, Phys. Rev. **E62** (2000) 5818-5829.
39. N.P. Barradas, R. Patrício, A. Vieira, *RBS without humans*, IBA15, Nucl. Instr. and Methods **B190** (2002) 231-236

40. P.Bauer, E.Steinbauer, J.P.Biersack, *The width of an RBS spectrum: influence of plural and multiple scattering*, Nucl. Instr. and Methods **B64** (1992) 711-715
41. P.Bauer, E.Steinbauer, J.P.Biersack, *RBS beyond the single scattering model*, Nucl. Instr. and Methods **B79** (1993) 443-445
42. R.T.Bayes, *Essay toward solving a problem in the doctrine of chance*, Phil.Trans.Roy.Soc. **53** (1763) 370
43. A.Belson, D.Brasted, C.Dawes, S.Mashford, H.Sunnucks, J.S.Sharpe, C.N.McKinty, M.Kerford, M.A.Lourenço, A. Kewell, T.Butler, K.P.Homewood, C.Jeynes, R.P.Webb, K.J.Reeson Kirkby, *Ion Beam Synthesised FeSi₂ – development of band gap and structure during annealing*, CREST Masterclass project: Presented at ESPRIT Advanced Research Initiative in Microelectronics (MEL-ARI) Athens, October 1999
44. A.A.Bettiol, D.N.Jamieson, S.Prawer, M.G.Allen, *Ion beam induced luminescence from diamond and other crystals from a nuclear microbeam*, Nucl. Instr. and Methods **B85** (1994) 775-779
45. M.Bianconi, F.Abel, J.C.Banks, A.Climent Font C.Cohen, B.L.Doyle, R.Lotti, G.Lulli, R.Nipoti, I.Vickridge, D.Walsh, E.Wendler, *The Si surface yield as a calibration standard for RBS*, Nucl. Instr. and Methods **B161-163** (2000) 293-296
46. N.Bibic, S.Dhar, M. Milosavljević, K.Removic, L.Rissanen, K.P.Lieb, *Interface mixing in Ta/Si bilayers with Ar ions*, Nucl. Instr. and Methods **161-163** (2000) 1011-1015
47. M. Blaauw, J. L. Campbell, S. Fazinić, M. Jakšić, I. Orlic, P. Van Espen, *The 2000 IAEA intercomparison of PIXE spectrum analysis software*, Nucl. Instr. and Methods **B189** (2002) 113-122
48. P.Børgeesen, R.Behrish, B.M.U.Scherzer, *Depth profiling by ion-beam spectrometry*, Appl.Phys.**A27** (1982) 183-195
49. G. Boudreault, C. Jeynes, E. Wendler, A.Nejim, R.P.Webb, U. Wätjen, *Accurate RBS measurement of ion implant doses in silicon*, Surf.Interface Analysis **33** (2002) 478-486
50. W.H.Bragg, R.Kleeman, *On the α Particles of Radium, and their Loss of Range in passing through various Atoms and Molecules*, Phil.Mag. **10** (1905) S318-340
51. M.B.H.Breese, A.Amaku, P.R.Wilshaw, *A comparison between the use of EBIC and IBIC microscopy for semiconductor defect analysis*, Nucl. Instr. and Methods **B136-138** (1998) 1355-1360
52. M.B.H.Breese, P.J.C.King, D.G.de Kerckhove, *Strain and defect imaging using a nuclear microprobe*, Nucl. Instr. and Methods **B136-138** (1998) 23-34
53. D.K.Brice, *Theoretical analysis of the energy spectra of backscattered ions*, Thin Solid Films **19** (1973) 121-135
54. J.W.Butler, *Criteria for validity of Rutherford scatter analysis*, Nucl. Instr. and Methods **B45** (1990) 160-165
55. A.Cappellani, J.L.Keddie, N.P.Barradas, S.M.Jackson, *Processing and characterisation of sol-gel deposited Ta₂O₅ and TiO₂- Ta₂O₅ dielectric thin films*, Solid State Electronics **43** (1999) 1095-1099
56. J.D.Carey, R.D.Forrest, R.U.A.Khan, R.R.P.Silva, *Influence of sp(2) clusters on the field emission properties of amorphous carbon thin films*, Appl.Phys.Lett. **77** (2000) 2006-2008
57. J.D.Carey, R.R.P.Silva, *Conditioning of hydrogenated amorphous carbon thin films for field emission via current stressing*, Appl.Phys.Lett. **78** (2001) 347-349
58. W.K.Chu, J.W.Mayer, M.-A.Nicolet, *Backscattering Spectrometry* (Academic Press, New York, 1978)

59. P.J.Cumpson, *Angle-resolved XPS and AES: depth resolution limits and a general comparison of properties of depth-profile reconstruction methods*, J.Elec.Spec.& Related Methods **73** (1995) 25-52
60. J.A.Davies, W.N.Lennard, I.V.Mitchell, *Pitfalls in Ion Beam Analysis*, Chapter 12 in IBA Handbook (Tesmer & Nastasi, 1995).
61. L.R.Doolittle, *A semi-automatic algorithm for RBS analysis*, Nucl. Instr. and Methods **B15** (1986) 227-231
62. K.H.Ecker, U. Wätjen, A.Berger, L.Persson, W. Pritzkow, M. Radtke, H. Rieseemeier, *RBS, SY-XRF, INAA and ICP-IDMS of antimony implanted in silicon – a multi-method approach to characterize and certify a reference material*, Nucl. Instr. and Methods **B188** (2002) 120-125
63. W.Eckstein, M.Mayer, *Rutherford backscattering from layered structures beyond the single scattering model*, Nucl. Instr. and Methods **B153** (1999) 337-344
64. R.D.Edge, *RBS microscopic "Tomography"*, IEEE Trans.Nucl.Sci. **NS-30** (2) (April 1983) 1685-1687
65. R.D.Edge, *Element distributions at depth from an iterative analysis of RBS spectra*, Nucl. Instr. and Methods **B35** (1988) 309-314
66. L.C.Feldman, J.W.Mayer, S.T.Picraux, *Materials Analysis by Ion Channeling* (Academic Press, New York, 1982)
67. R.Fischer, M.Mayer, W.von der Linden, V.Dose, *Enhancement of the energy resolution in ion-beam experiments with the maximum-entropy method*, Phys.Rev.E **55** (June 1997) 6667- 6673
68. R.Fischer, M.Mayer, W.von der Linden, V.Dose, *Energy resolution enhancement in ion beam experiments with Bayesian probability theory*, Nucl. Instr. and Methods **B136-8** (1999) 1140-1145
69. A.Garrett, *Ockham's Razor*, Physics World **4** (May 1991) 39-42
70. H.Geiger, *The Scattering of the α - Particles by Matter*, Royal Society Proceedings **A83** (1909) 492-504
71. H.Geiger, E.Marsden, *On a Diffuse Reflection of the α - Particles*, Royal Society Proceedings **A82** (1909) 495-500
72. H.Geiger, E.Marsden, *On the Laws of Deflexion of α Particles through Large Angles*, Phil.Mag., **25** (1913) 604-623
73. S.Geman, D.Geman, *Stochastic relaxation, Gibbs distributions, and the Bayesian restoration of images*, IEEE Trans. Pattern Analysis & Machine Intelligence **6** (1984) 721-741
74. W.R.Gilks, S.Richardson (eds.), *Markov Chain Monte Carlo* (Chapman & Hall, London, 1996)
75. G.W.Grime, M.D.Dawson, *Recent developments in data acquisition and processing on the Oxford Scanning proton microprobe*, Nucl. Instr. and Methods B104 (2002) 107-113
76. G.Götz, K.Gärtner (eds.), *High Energy Ion Beam Analysis of Solids*, (Akademie-Verlag, Berlin, 1988)
77. A.F.Gurbich, *On the origin of the low energy tail in charged particle spectra*, Nucl. Instr. and Methods **A364** (1995) 496-500
78. A.F.Gurbich, *Evaluation of non-Rutherford proton elastic scattering cross-section for oxygen*, Nucl. Instr. and Methods **B129** (1997) 311-316
79. A.F.Gurbich, *Evaluation of non-Rutherford proton elastic scattering cross-section for carbon*, Nucl. Instr. and Methods **B136-138** (1998) 60-65
80. A.F.Gurbich, *Evaluation of non-Rutherford proton elastic scattering cross-section for silicon*, Nucl. Instr. and Methods **B145** (1998) 578-583

81. A.F.Gurbich, *Proton elastic scattering cross-section for carbon: confrontation of theory and experiment*, Nucl. Instr. and Methods **B152** (1999) 403-405
82. F.Harbsmeier, W.Bolse, A.-M.Flank, *Solid state reaction in Si-C multilayers induced by ion bombardment*, Nucl. Instr. and Methods **166-167** (2000) 385-389
83. M.A.Harry, G.Curello, M.S.Finney, K.J.Reeson, B.J.Sealy, *Structural properties of ion beam synthesised iron-cobalt silicides*, J.Phys.D **29** (1996) 1822-1830
84. J.-P.Hirvonen, *Nuclear Reaction Analysis: Particle-Gamma Reactions*, in Tesmer & Nastasi (eds), Handbook (1995) ch.7
85. S.M.Jackson, *Optical characterisation of cubic silicon carbide*, PhD Thesis, University of Surrey, September 1998
86. C.Jeynes, Z.H.Jafri, R.P.Webb, M.J.Ashwin, A.C.Kimber, *Accurate RBS measurements of the In content of InGaAs thin films*, Surf.Interface Anal. **25** (1997) 254-260
87. C.Jeynes, N.P.Barradas, M.J.Blewett, R.P.Webb, *Improved ion beam analysis facilities at the University of Surrey*, Nucl. Instr. and Methods **B136-138** (1998) 1229-1234
88. C.Jeynes, N.P.Barradas, H.Rafla-Yuan, B.P.Hichwa, R.Close, *Accurate depth profiling of complex optical coatings*, Surface & Interface Analysis **30** (2000) 237-242
89. C. Jeynes, N.P.Barradas, J.R.Wilde, A.L.Greer, *Composition of TaNiC thick films using SimAnn: Elastic Backscattering Spectrometry*, Nucl. Instr. and Methods **B161-163** (2000) 287-292
90. C.Jeynes, G.G.Rozenburg, S.P.Speakman, J.H.G.Steinke, *A microbeam RBS analysis of low temperature direct-write inkjet deposited copper*, Nucl. Instr. and Methods **B188** (2002) 141-145
91. S.A.E.Johanssen, J.L.Campbell, *PIXE: A Novel Technique for Elemental Analysis* (John Wiley & Sons, Chichester, 1988)
92. B.Jouffrey, J.Svejcar (eds), *Microstructural Investigation and Analysis* (Wiley, 2000)
93. S.Kirkpatrick, C.D.Gelatt Jr., M.P.Vecchi, *Optimization by Simulated Annealing*, Science **220** (1983) 671-680
94. G. Konac, S. Kalbitzer, C. Klatt, D. Niemann and R. Stoll, *Energy loss and straggling of H and He ions of keV energies in Si and C*, Nucl. Instr. and Meth. **B136-138** (1998) 159-165
95. E.Kótai, *Computer methods for analysis and simulation of RBS and ERDA spectra*, Nucl. Instr. and Methods **B85** (1994) 588-596
96. D.L.Kogan, A.M.Kazancev, L.E.Kuzmin, *BEAM EXPERT - integrated software for nuclear analysis*, Nucl. Instr. and Methods **B88** (1994) 495-498
97. W.A.Lanford, B.Anderberg, H.Enge, B.Hjorvarsson, *Compact broad range magnetic spectrometer for use in ion beam analysis*, Nucl. Instr. and Methods **B136-138** (1998) 1177-1182
98. P.M.Lee, *Bayesian Statistics: an Introduction*, (2nd ed.: Arnold, London, 1997)
99. W.N.Lennard, private communication, 2nd February 2000
100. W.N.Lennard, G.R.Massoumi, P.F.A.Alkemade, I.V.Mitchell, N.S.McIntyre, R.D.Davison, *Deuterium depth distribution investigations in Zr and ZrO₂*, Nucl. Instr. and Methods **B73** (1993) 203-213
101. W.N.Lennard, G.R.Massoumi, T.W.Simpson, I.V.Mitchell, *Improved stoichiometry measurements using ⁴He backscattering: experiment and simulation*, Nucl. Instrum. and Methods **B152** (1999) 370-376
102. W.N.Lennard, S.Y.Tong, G.R.Massoumi, L.Wong, *On the calibration of low energy ion accelerators*, Nuclear Instr. & Methods **B45** (1990) 281-284
103. D.Leong, M.A.Harry, K.J.Reeson, K.P.Homeood, *A silicon/iron disilicide light emitting diode operating at a wavelength of 1.5 μm*, Nature **387** (1997) 686-688

104. S.C.Liew, K.K.Loh, S.M.Tang, *Application of an iterative maximum-likelihood algorithm in PIXE depth profiling of trace elements*, Nucl. Instr. and Methods **B85** (1994) 621-626
105. E.Lifshin (ed), *X-ray Characterization of Materials* (Wiley, 1999)
106. K.K.Loh, C.H.Sow, K.H.Tan, H.S.Tan, S.M.Tang, I Orlic, T.Osipowitz, *Measurement of phosphorus content in silica layers*, Nucl. Instr. and Methods **B75** (1993) 364-366
107. K.G.Malmqvist (ed.), *Proceedings of the 8th Int. Conf. on Particle Induced X-ray Emission and its Applications* (Lund, June 14-18, 1998) Nucl. Instr. and Methods **B150(1-4)** (1999)
108. J.Malléol, J.-P.Gorse, C.Jeynes, O.Dupont, J.Keddie, *Origins and Effects of a Surfactant Excess at the Surface of Waterborne Acrylic Pressure Sensitive Adhesives*, Langmuir **18** (2002) 4478-4487
109. N.Marin, Y.Serruys, P.Calmon, *Extraction of lateral non-uniformity statistics from Rutherford backscattering spectra*, Nucl. Instr. and Methods **B108** (1996) 179-187
110. P.K.Marriott, M.Jenkin, C.Jeynes, N.P.Barradas, R.P.Webb, B.J.Sealy, *Rapid accurate automated analysis of complex ion beam analysis data*, **CP475**, Applications of Accelerators in Research and Industry (eds. J.L.Duggan, I.L.Morgan, Woodbury, New York: AIP, 1999), pp592-595
111. P.K.Marriott, M.Jenkin, C.Jeynes, *The Analysis of Rutherford Backscattering Spectra*, J.Roy.Stat.Soc.C, Appl. Statistics (in preparation, 2002)
112. N.Metropolis, A.W.Rosenbluth, M.N.Rosenbluth, A.H.Teller, E.Teller, *Equation of state calculations by fast computing machines*, J.Chem.Phys. **21** (1953) 1087-1092
113. J.W.Mayer, E.Rimini (eds.), *Ion Beam Handbook for Materials Analysis*, (Academic Press, New York, 1977). Known as the "Catania" Handbook, it includes a section on PIXE.
114. J.W.Mayer, J.F.Ziegler (eds.), *Proceedings of the International Conference on Ion Beam Surface Layer Analysis*, Thin Solid Films **19** (1973)
115. M.Mayer, *SIMNRA User's Guide*, Technical Report IPP 9/113, Max-Planck-Institut für Plasmaphysik, Garching, Germany (1997)
116. M.Milosavljević, N.Bibic, D.Perusko, C.Jeynes, U.Bangert, *The effects of implanted arsenic on Titanium silicide formation*, in: Special defects in semiconducting materials ed.R.P.Agarwala, Solid State Phenomena **71** (2000) 142-172 (Scitech publications, Switzerland, 1999)
117. M.Milosavljević, N.Bibic, K.P.Homewood, C.Jeynes, *Formation of β -FeSi₂ by combining ion beam mixing and thermal processing*, Thin Solid Films (in press, 2002)
118. W.Möller *et al* (eds), *Proceedings of the 14th Int. Conf. on Ion Beam Analysis* (Dresden, Sept. 1999) Nucl. Instr. and Methods **B161-163** (2000)
119. R.Nagel, A.G.Balogh, *Atomic transport in metal/ceramic interfaces under heavy ion irradiation*, Nucl. Instr. and Methods **B156** (1999) 135-142
120. R.Nagel, H.Hahn, A.G.Balogh, *Diffusion processes in metal/ceramic interfaces under heavy ion irradiation*, Nucl. Instr. and Methods **B148** (1999) 930-935
121. D.Niemann, G.Konac, S.Kalbitzer, *Stopping power measurements of ¹H, ⁴He, and ¹⁴N in the energy range of 0.02 - 1 MeV/amu*, Nucl. Instr. and Methods **B118** (1996) 11-18
122. H. Niwa, S. Nakao, K. Saitoh, *Application of HI-RBS to compositional analysis of thin films*, Nucl. Instrum. Methods B 136-138 (1998) 297-300
123. J.Padayachee, V.M.Prozesky, W.von der Linden, M.S.Nkwinika, V.Dose, *Bayesian PIXE background subtraction*, NIM **B150** (1999) 129-135
124. R.S.Payne, A.S.Clough, P.Murphy, P.J.Mills, *Use of the D(³He,p)⁴He reaction to study polymer diffusion in polymer melts*, Nucl. Instr. and Methods **B42** (1989) 130-134

125. W.H.Press, S.A.Teukolsky, W.T.Vetterling, B.P.Flannery, *Numerical Recipes in Fortran*, (2nd ed., Cambridge University Press, Cambridge, 1992) p.438
126. V.M.Prozesky, J.Padayachee, R.Fischer, W.von der Linden, V.Dose, C.G.Ryan, *The use of maximum entropy and Bayesian techniques in nuclear microprobe applications*, Nucl.Instruments & Methods **B130** (1997) 113-117
127. V.M.Prozesky, J.Padayachee, R.Fischer, W.von der Linden, V.Dose, R.A.Weller, *Bayesian techniques and the principle of maximum entropy in ion beam analysis applications*, Nucl.Instruments & Methods **B136-8** (1999) 1146-1151
128. V.M.Prozesky, W.J.Przybyłowicz, C.A.Pineda (eds), *Proceedings of the 6th Int. Conf. Nuclear Microprobe Technology and its Applications* (Cape Town, October 11-16, 1998) Nucl. Instr. and Methods **B158(1-4)** (1999)
129. Yu.P.Pyt'ev, *Reduction problems in experimental investigations*, Mathematics of the USSR-Sbornik **120** (1983) (in Russian: translation in Math.USSR Sbornik **48**, 1984, 237-272)
130. E.Rauhala, *Energy Loss*, in Tesmer & Nastasi (eds), *IBA Handbook* (1995) ch.2
131. M.A.Respaldiza, J.Gómez-Camacho (eds), *Applications of Ion Beam Analysis to Arts and Archaeometry* (Universidad de Sevilla, 1997)
132. L.S.Riley, S.Hall, J.Harris, J.Fernandez, B.Gallas, A.G.R.Evans, J.F.Clark, J.Humphrey, R.T.Murray, C.Jeynes, *SiGe nMOSFETs with gate oxide grown by low temperature plasma oxidation*, Microelec.Eng. **48** (1999) 227-230
133. S.Rodil, N.A.Morrison, W.I.Milne, J.Robertson, V.Stolovan, D.N.Jayawardane, *Deposition of carbon nitride films using an electron cyclotron wave resonance plasma source*, Diamond & Related Materials **9** (2000) 524-529
134. E.Rokita, B.Maj, P.H.A.Mutsaers, M.J.A. de Voigt, *The use of the maximum entropy method for the improvement of the spacial resolution of micro-PIXE maps*, Nucl.Instruments & Methods **B130** (1997) 138-143
135. G.G.Rozenberg, E.Bresler, S.P.Speakman, C.Jeynes, J.H.G.Steinke, *Patterned low temperature copper-rich deposits using inkjet printing*, Appl.Phys.Lett. (accepted)
137. J.Ross, N.P.Barradas, M.P.Hill, C.Jeynes, P.Morrissey, J.F.Watts, *Rutherford backscattering spectrometry and computer simulation for the in-depth analysis of chemically modified poly(vinylidene fluoride)*, J.Mat.Sci. **36** (2001) 1-8
138. E.Rutherford, *The Scattering of α and β Particles by Matter and the Structure of the Atom*, Phil.Mag. **21** (1911) 669-688
139. C.G.Ryan, E.van Achterbergh, C.J.Yeats, S.L.Drieberg, G.Mark, B.M.McInnes, T.T.Win, G.Cripps, G.F.Suter, *Quantitative, high sensitivity, high resolution, nuclear microprobe imaging of fluids, melts and minerals*, Nucl.Instruments & Methods **B188** (2002) 18-27
140. M.P.Seah, D.David, J.A.Davies, C.Jeynes, C.Ortega, C.Sofield, G.Weber, *An inter-comparison of absolute measurements of the oxygen and tantalum thickness of Ta₂O₅ reference materials BCR 261 by six laboratories*, Nucl.Instruments & Methods **B30** (1988) 140-151
141. Y.Serruys, *Rational smoothing applied to Rutherford backscattering spectrometry*, Nucl. Instr. and Methods **B44** (1990) 473-478
142. Y.Serruys, *Simulation of Rutherford backscattering spectra: "retrograde" method*, Nucl. Instr. and Methods **B61** (1991) 221-225
143. Y.Serruys, J.Tirara, P.Calmon, *Concentration profile reconstitution from Rutherford backscattering spectra*, Nucl. Instr. and Methods **B74** (1993) 565-572
144. V. S. Shorin, A. N. Sosnin, *RBS spectra for thin films with surface roughness*, Nucl. Instrum. Methods B **72** (1992) 452-456

145. A.Simon, F.Pászti, I.Uzonyi, A.Manuaba, Á.Z.Kiss, I.Rajta, *Observation of surface topography using an RBS microbeam*, Nucl. Instr. and Methods **B136-138** (1998) 344-349
146. J.Slotte, A.Laakso, T.Ahlgren, E.Rauhala, R.Salonen, J.Räisänen, A.Simon, I.Uzonyi, Á.Z.Kiss, E.Somorjai, *Influence of surface topography on depth profiles obtained by Rutherford backscattering spectrometry*, J.Appl.Phys.**87** (2000) 140-143
147. G.B.Sorkin, *Efficient simulated annealing on fractal energy landscapes*, Algorithmica **6** (1991) 367-418
148. A.L.Stepanov, D.E.Hole, P.D.Townsend, *Reflectance of the dielectric layers containing metal nanoparticles for by ion implantation*, J.Non-Cryst.Solids **244** (1999) 275-279
149. E.Szilágyi, F.Pászti, *Theoretical calculation of the depth resolution of IBA methods*, Nucl. Instr. and Methods **B85** (1994) 616-620
150. E.Szilágyi, F.Pászti & G.Amsel, *Theoretical approximations for depth resolution calculations in IBA methods*, Nucl. Instr. and Methods **B100** (1995) 103-121
151. C.J.Tavares, L.Rebouta, E.Alves, N.P.Barradas, J.Pacaud, J.P.Riviére, *Study of roughness in TiAlN/Mo multilayer structures*, Nucl. Instrum. Methods **B188** (2002) 90-95
152. J.R.Tesmer, M.Nastasi (eds), *Handbook of Modern Ion Beam Analysis* (Materials Research Society, Pittsburgh, 1995). Does not include PIXE (see Mayer & Rimini).
153. H.Timmers, R.G.Elliman, private communications, October 1999
154. A.Tzitzinou, P.M.Jenneson, A.S.Clough, J.L.Keddie, J.R.Lu, P.Zhdan, K.E.Treacher, R.Satgaru, *Surfactant concentration and morphology at the surfaces of acrylic latex films*, Progress in Organic Coatings **35** (1999) 89-99
155. J.Tirara, Y.Serruys, P.Trocellier, *Forward Recoil Spectrometry* (Plenum Press, New York, 1996)
156. S.J.Toal, H.S.Reehal, S.J.Webb, N.P.Barradas, C.Jeynes, *Structural analysis of nanocrystalline SiC thin films grown on Si by ECR plasma CVD*, Appl.Surface Sci. **138-139** (1999) 424-428
157. S.Uchikoga, D.F.Lai, J.Robertson, W.I.Milne, N.Hatzopoulos, R.A.Yankov, M.Weiler, *Low-temperature anodic oxidation of silicon using a wave resonance plasma source*, Appl.Phys.Lett. **75** (1999) 725-727
158. A.Veloso, P.P.Freitas, P.Wei, N.P.Barradas, J.C.Souares, B.Almeida, J.B.Sousa, *Magnetoresistance enhancement in specular, bottom-pinned, Mn₈₃Ir₁₇ spin valves with nano-oxide layers*, Appl.Phys.Lett. **77** (2000) 1020-1022
159. A. Vieira and N. P. Barradas, *Neural network analysis of Rutherford backscattering data*, Nucl. Instrum. Methods **B170** (2000) 235-238
160. A. Vieira, N. P. Barradas, *Composition of NiTaC films on Si using neural networks analysis of elastic backscattering data*, Nucl. Instrum. Methods **B174** (2001) 367-372
161. A. Vieira, N. P. Barradas, C. Jeynes, *Error performance analysis of Artificial Neural Networks applied to Rutherford backscattering data*, Surf. Interface Analysis **31** (2001) 35-38.
162. G.Vizkelethy, *Nuclear Reaction Analysis: Particle-Particle Reactions*, in Tesmer & Nastasi (eds), Handbook (1995) ch.6
163. A.Vonsovici, G.T.Reed, A.G.R.Evans, F.Namavar, *Loss measurements for β -SiC-on-insulator for high-speed silicon-based photonic devices*, SPIE Conf.on Si-based Optoelectronics (San Jose, Calif., Jan.1999), SPIE **3630** (1999) 115-124
164. A.M.Vredenberg, A.Polman, P.A.Stolk, E.Snoeks, M.L.Brongersma (eds), *Proceedings of the 11th Int. Conf. Ion Beam Modification of Materials* (Amsterdam, Aug 31 - Sep 4, 1998) Nucl. Instr. and Methods **B148(1-4)** (1999)

165. F.Watt, G.W.Grime, Principles and Applications of High-Energy Ion Microbeams (Adam Hilger, Bristol, 1987)
166. Y.A.Wilks, B.M.Slator, L.M.Guthrie, *Electric Words: Dictionaries, Computers, Meanings* (MIT Press, Cambridge Mass., 1996)
167. J.S.Williams, W.Möller, On the determination of optimum depth-resolution conditions for Rutherford backscattering analysis, *Nucl. Instr. and Methods* **157** (1978) 213-221
168. J.M.Walls (ed), *Methods of Surface Analysis* (Cambridge University Press, 1989)
169. U.Wätjen, private communication, 9th February 2000
170. U.Wätjen, H.Bax, Bi-implanted silicon reference material revisited: uniformity of the remaining batch, *Nucl. Instr. and Methods* **B85** (1994) 627-632
171. U.Wätjen, H.Bax, P.Rietveld, *Evaporated and Implanted Reference Layers for Calibration in Surface Analysis*, *Surface & Interface Analysis* **19** (1992) 253-258
172. A.S.Way, C.Jeynes, R.P.Webb, Measurement of lateral stress in argon implanted thin gold films using quartz resonator techniques, *Nucl. Instr. and Methods* **148** (1999) 238-241
173. E.Wendler, C.Jeynes, R.P.Webb, N.P.Barradas, R.Thompson, Richard Smith, *Hydrogen isotope profiling of functionalised polystyrene blends using RBS/ERD and RBS/NRA with Simulated Annealing analysis*, 11th AINSE Conference on Nuclear Techniques of Analysis, Lucas Heights, (Australia) 24-26 November 1999
174. Z. Xie, E. Z. Luo, H. B. Peng, B. R. Zhao, G. D. Hu, I. H. Wilson, J. B. Xu, L. H. Zhao, *Studies of leakage current inhomogeneity of Pb(Zr, Ti)O₃/YBa₂Cu₃O_x heterostructures on a nanometer scale*, *Journal of Non-Crystalline Solids* **254** (1999) 112-117
175. C.Yang, N.P-O Homman, L.Johanssen, K.G.Malmqvist, *Microcharacterizing zircon mineral grain by ionoluminescence combined with PIXE*, *Nucl. Instr. and Methods* **B85** (1994) 808-814
176. W.T.Young, S.R.P.Silva, J.V.Angueta, J.M.Shannon, K.P.Homewood, B.J.Sealy, *Low temperature growth of gallium nitride*, *Diamond and Related Materials* **9** (2000) 456-459
177. I.M.Yesil, W.Assmann, H.Huber, K.E.G.Löbner, *Simulation of surface roughness effects in ERDA*, *Nucl. Instrum. Methods* **B136-138** (1998) 623-627
178. J.F.Ziegler, J.P.Biersack, U.Littmark, *The Stopping and Ranges of Ions in Solids* (Pergamon Press, New York, 1985)
179. Z.Zhang, S.Cardoso, P.P.Freitas, P.Wei, N.Barradas (sic), J.C.Soares, *Annealing effect of magnetic tunnel junctions with one FeO_x layer inserted at the Al₂O₃/CoFe interface*, *Appl.Phys.Lett.* **78** (2001) 2911-2913